THE ASTROPHYSICAL JOURNAL, 468:121–138, 1996 September 1

APM $Z \geq 4$ QSO SURVEY: SPECTRA AND INTERVENING ABSORPTION SYSTEMS

L. J. STORRIE-LOMBARDI[1] AND R. G. MCMAHON
Institute of Astronomy Madingley Road, Cambridge CB3 0HA, UK; lisa@ociw@edu; rgm@ast.cam.ac.uk
M. J. IRWIN
Royal Greenwich Observatory Madingley Road, Cambridge CB3 0EZ, UK; mike@ast.cam.ac.uk
AND
C. HAZARD
University of Pittsburgh, Pittsburgh, PA 15260; and Institute of Astronomy; hazard@ast.cam.ac.uk

Received 1995 October 11; accepted 1996 March 15

ABSTRACT

The APM multicolor survey for bright $z > 4$ objects, covering 2500 deg^2 of sky to $m_r \sim 19$, resulted in the discovery of 31 quasars with $z \gtrsim 4$. High signal-to-noise optical spectrophotometry at 5 Å resolution has been obtained for the 28 quasars easily accessible from the northern hemisphere. These spectra have been surveyed to create new samples of high-redshift Lyman-limit systems, damped Lyα absorbers, and metal absorption systems (e.g., C IV and Mg II). In this paper we present the spectra, together with line lists of the detected absorption systems. The QSOs display a wide variety of emission- and absorption-line characteristics, with five exhibiting broad absorption lines and one with extremely strong emission lines (BR 2248 − 1242). Eleven candidate damped Lyα absorption systems have been identified covering the redshift range $2.8 \leq z \leq 4.4$ (eight with $z > 3.5$). An analysis of the measured redshifts of the high-ionization emission lines with the low-ionization lines shows them to be blueshifted by 430 ± 60 km s^{-1}. In a previous paper (by Storrie-Lombardi et al.) we discussed the redshift evolution of the Lyman limit systems cataloged here. In subsequent papers we will discuss the properties of the Lyα forest absorbers and the redshift and column density evolution of the damped Lyα absorbers.

Subject headings: quasars: absorption lines — quasars: emission lines — quasars: general

1. INTRODUCTION

Many QSOs have now been discovered beyond redshifts of 4, and they provide powerful probes for exploring these early epochs. They are the youngest objects known in the universe, and it is likely that they flag regions where galaxy formation is very active. Their host galaxies are probably still forming, and they may occur in the exceptional "5 σ" peaks in the matter distribution of the early universe (Efstathiou & Rees 1988). Observational information from this epoch yields constraints on galaxy formation theories and clues for better understanding of the astrophysics of galaxy formation and evolution.

In addition to being of intrinsic interest themselves, bright high-redshift QSOs are particularly valuable as probes of the intervening gas clouds and galaxies superimposed on their spectra in absorption. The study of these absorption systems provides information about the formation and evolution of galaxies over most of the age of the universe. Neutral hydrogen (H I) absorption can be detected over a staggering 10 orders of magnitude from the Lyα forest region with the weakest detectable lines having a column density $N_{\rm H\,I} \sim 10^{12}$ atoms cm^{-2}, up to the damped Lyα absorbers with $N_{\rm H\,I} \sim 10^{21}$. The rich zoo of these absorbers, in addition to those produced by heavier elements such as carbon, silicon, oxygen, and magnesium, are illuminated along a QSO line of sight, leaving their imprint as absorption in the QSO continuum. Study of the Lyα forest ($12 \lesssim \log N_{\rm H\,I} \lesssim 17$) yields important information about the intergalactic medium and the background ionizing flux at high redshifts (e.g., Hunstead et al. 1986; Carswell et al. 1987; Bajtlik, Duncan, & Ostriker 1988; Williger et al. 1994). Lyman-limit systems ($\log N_{\rm H\,I} \gtrsim 17$) provide a means of directly studying the evolution of galaxies over the redshift range $0.1 < z < 5$ (e.g., Sargent, Steidel, & Boksenberg 1989; Lanzetta et al. 1991; Storrie-Lombardi et al. 1994; Stengler-Larrea et al. 1995). The absorbers detected via the damped Lyα lines they produce ($\log N_{\rm H\,I} \gtrsim 20$) show features consistent with an early phase of galactic evolution and are widely believed to be the progenitors of spiral galaxies like our own (e.g., Wolfe et al. 1986, 1995; Wolfe 1987; Fall, Pei, & McMahon 1989; Pettini, Boksenberg, & Hunstead 1990; Rauch et al. 1990; Lanzetta et al. 1991; Lanzetta, Wolfe, & Turnshek 1995).

The APM Color Survey for $z > 4$ QSOs was undertaken to find bright ($m_R \lesssim 19$) quasars with redshifts $4 \lesssim z \lesssim 5$ (Irwin, McMahon, & Hazard 1991). The aim of the program was to find a large sample of QSOs for both intrinsic and absorption-line studies. The survey covers approximately 2500 square degrees of sky from the equatorial region of the UK Schmidt Telescope (UKST) B_J, R, I Survey with $|b| > 30°$ and declination range +3 to −17.5. High signal-to-noise optical spectrophotometry at 5 Å resolution covering the wavelength region 3500–9000 Å were obtained for all the QSOs discovered in the APM Color Survey that are accessible using the William Herschel Telescope (WHT) (28 of 31 objects). In addition, spectra were obtained at 5 Å resolution of three high-redshift radio-selected QSOs (Hook et al. 1995; McMahon et al. 1996). The spectra have been utilized to discover Lyman-limit, damped Lyα, and metal absorption systems (e.g., C IV and Mg II).

The results and analyses from these studies are presented in a series of papers. In this paper we present the spectra, together with a list of accurate redshift determinations of

---

[1] Postal address: Carnegie Observatories, 813 Santa Barbara Street, Pasadena, CA 91101.

TABLE 1

WHT ISIS OBSERVATIONS LOG

QSO	Date (UT)	Exposure (s)	Arm	Slit (arcsec)
BR 0019−1522	1992 Oct 4	2700	R/B	1.5
		600	R/B	5
BRI 0103+0032	1993 Aug 21	2700	R	1.5
		3000	B	1.5
		300	R/B	5
BRI 0151−0025	1993 Aug 21	2700	R	1.5
		3000	B	1.5
		300	R/B	5
BRI 0241−0146	1993 Aug 21	1800	R/B	1.5
		300	R/B	5
BR 0245−0608	1993 Aug 21	2700	R	1.5
		3000	B	1.5
		300	R/B	5
BR 0351−1034	1993 Aug 21	900	R/B	1.5
	1993 Sep 20	2700	R	1.5
		2800	B	1.5
BR 0401−1711	1995 Feb 02	3600	R/B	1.5
BR 0945−0411	1992 Apr 24	2700	R/B	1.5
		300	R	5
BR 0951−0450	1992 Apr 25	2700	R/B	1.5
		300	R	5
BRI 0952−0115	1992 Apr 24	900	R	1.5
		1000	B	1.5
		300	R	5
BRI 1013+0035	1992 Apr 24	2700	R/B	1.5
		300	R	5
BR 1033−0327	1993 Apr 17	2700	R/B	1.5
		600	R	5
BRI 1050−0000	1992 Apr 25	1800	R/B	1.5
		300	R	5
BRI 1108−0747	1992 Apr 25	1800	R/B	1.5
		300	R	5
BRI 1110+0106	1992 Apr 25	1800	R/B	1.5
		300	R	5
BRI 1114−0822	1993 Apr 11	2700	R	1.5
		3000	B	1.5
		300	R	5
BR 1117−1329	1992 Apr 24	1200	R/B	1.5
		300	R	5
BR 1144−0723	1992 Apr 25	1800	R/B	1.5
		300	R	5
BR 1202−0725	1992 Apr 23	2700	R	1.5
		2700	B	1.5
		1200	R	1.5
		300	R	5
	1993 Apr 17	2700	R	1.5
		3000	B	1.5
		600	R	5
BR 1302−1404	1993 Apr 17	1500	R/B	1.5
BRI 1328−0433	1993 Apr 17	2700	R	1.5
		3000	B	1.5
BRI 1335−0417	1992 Apr 25	2700	R/B	1.5
		300	R	5
BRI 1346−0322	1992 Apr 24	2700	R/B	1.5
		300	R	5
BRI 1500+0824	1992 Apr 25	2700	R/B	1.5
		300	R	5
GB 1508+5714	1993 Apr 17	2700	R	1.5
		3000	B	1.5
		600	R	5
MG 1557+0313	1992 Apr 25	2700	R/B	1.5
		300	R	5
GB 1745+6227	1993 Aug 21	2700	R	1.5
		3000	B	1.5
		600	R/B	5
BR 2212−1626	1993 Aug 21	2700	R	1.5
		3000	B	1.5
		450	R/B	5
BRI 2235−0301	1993 Aug 21	2700	R	1.5
		3000	B	1.5
		450	R/B	5
BR 2237−0607	1992 Oct 3	2700	R/B	1
BR 2248−1242	1993 Aug 21	2700	R	1.5
		3000	B	1.5
		300	R/B	5

the intrinsic QSO emission lines, a study of the velocity differences between high- and low-ionization emission lines, and the results of surveys for intervening absorption systems. Line lists for damped Lyα candidates, Lyman limit systems, and metal absorption systems are provided. The analysis of the redshift evolution of the Lyman limit systems was previously presented in Storrie-Lombardi et al. (1994). We will present a detailed analysis of the damped Lyα systems and the redshift evolution of their number density and column density distribution (Storrie-Lombardi, Irwin, & McMahon 1996a) and describe the implications derived from the damped Lyα survey for the evolution of the mass density of neutral gas with redshift and the implications for galaxy formation (Storrie-Lombardi, McMahon, & Irwin 1996b). Other papers will cover studies of the Lyα forest clouds at high redshift and the intrinsic properties of the QSOs. High-resolution studies of the Lyα forest region at $z > 4$ have been completed by Williger et al. (1994) and Wampler et al. (1996).

2. OBSERVATIONS

High signal-to-noise optical spectrophotometry at 5 Å resolution covering the wavelength range 3500−8800 Å was obtained with the 4.2 m William Herschel telescope of the Isaac Newton Group of telescopes in the Canary Islands. We used the ISIS double-spectrograph with typical integration times of 2700–3600 s. The spectrophotometry is accurate to within 5%–10%. ISIS is a double-beam spectrograph with arms optimized for blue and red light, mounted at the f/11 Cassegrain focus of the WHT. For this project the lowest dispersion was required, and gratings with 158 lines mm^{-1} and a dichroic to split the light at $\sim$5400 Å were used. This gives 2.71 Å pixel^{-1} in the red arm and 2.89 Å pixel^{-1} in the blue. The gratings were arranged so that the blue part of the spectrum was centered on 4600 Å and covered a range of 2950 Å while the red was centered on 7000 Å and covered a range of 3380 Å. The red and blue arm observations were carried out simultaneously. On the red arm an English Electric Valve (EEV) 1242 × 1152 CCD with 22.5 μm pixels was used as detector. On the blue arm a thinned Tektronix 1024 × 1024 CCD with 24 μm pixels was used. All the narrow-slit observations were taken with a slit width of $1''.5$ except for BR 2237−0607 ($1''$), and all were taken with the slit perpendicular to the horizon (at the parallactic angle). This slit orientation is used to minimize the effects of atmospheric differential refraction (Filippenko 1982).

Although the QSOs from the APM Color Survey are bright for high-redshift objects ($m_R < 19$), they were barely visible on the acquisition TV, so nearby offset stars ($m_R \sim$ 15–17) were acquired first. Blind-offsetting was then used to position the target object in the slit, and as a check the TV integration time was increased until the periphery of the QSO was visible in the slit. All observations were made with a long slit and the CCDs were windowed in the spatial direction to reduce the overhead due to readout time. The observations are summarized in Table 1.

3. DATA REDUCTION

The data were reduced using standard software from the IRAF[2] package. After the data were overscan, bias, and

---

[2] IRAF is distributed by the National Optical Astronomy Observatories, which is operated by the Association of Universities for Research in Astronomy, Inc. (AURA), under cooperative agreement with the

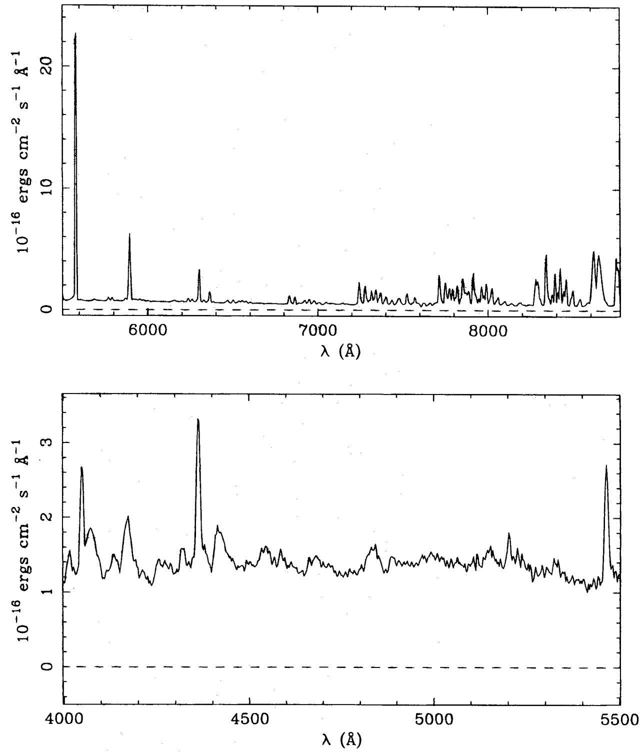

FIG. 1.—The 5 Å resolution flux calibrated sky spectrum from QSO BRI 1335−0417 taken with the red and blue arms of the ISIS spectrograph at the WHT.

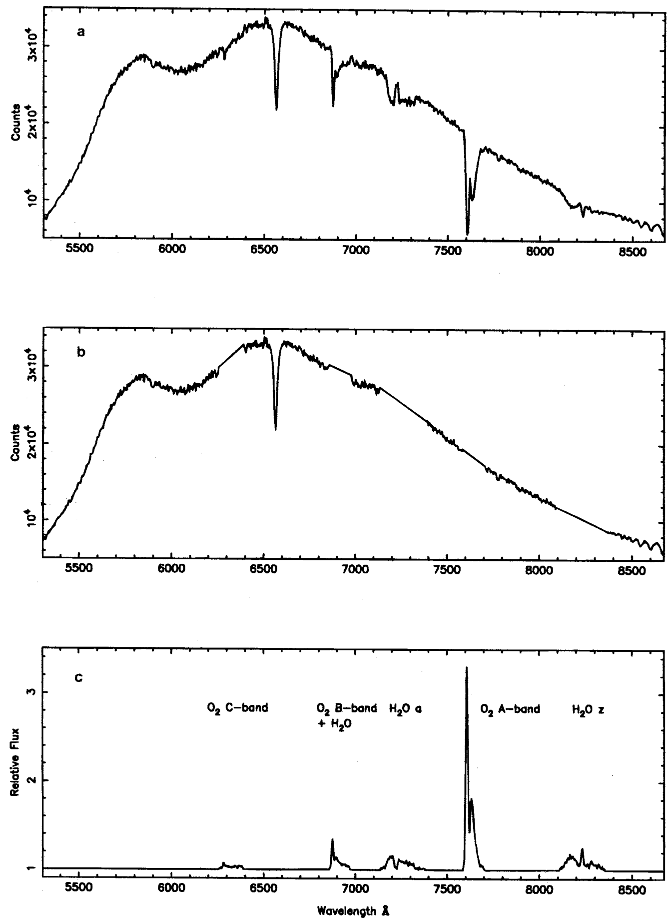

FIG. 3.—B star HD 13679: [B8, $m_V = 6.8$, exposure = 1 s, 1993 August 21, air mass = 1.056]; (*a*) wavelength-calibrated counts spectrum, (*b*) with atmospheric absorption features removed, and (*c*) the spectrum in (*a*) divided by the spectrum in (*b*). The absorption spectrum in (*c*) is then divided into the QSO spectra taken at a similar air mass to remove the atmospheric absorption features.

flat-field corrected they were extracted using the variance-weighted extraction in APALL. Typically the ISIS spectra curved by less than a pixel from one end of the chip to the other. APALL outputs the sky spectrum that was used for quick wavelength calibration at the telescope. A sample dark sky spectrum taken with ISIS is shown in Figure 1. CuNe+CuAr arcs were taken at intervals throughout the night to provide an accurate wavelength calibration. Emission lines were identified and a pixel-to-wavelength calibration curve was found by fitting a third-order Chebyshev polynomial to the calibration points in IDENTIFY. Typical rms residuals from the fit were 0.2 Å. The dispersion solution was applied to the extracted spectra, and they were put on a linear wavelength scale using DISPCOR.

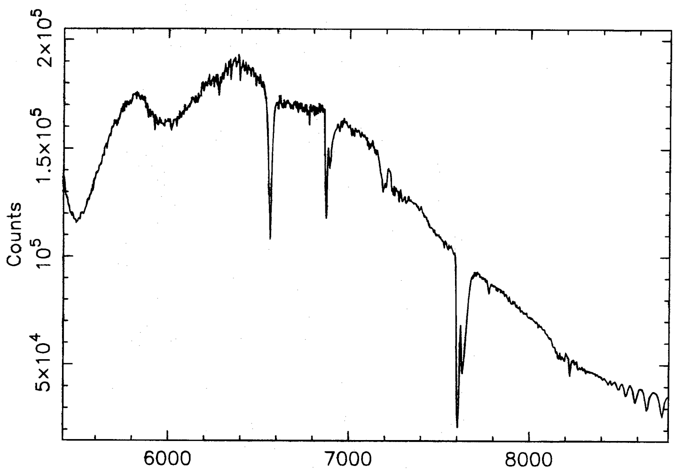

FIG. 2.—B star HR 4468: [B9.5, $m_V = 4.7$, exposure = 1 s, 1992 April 24, air mass = 1.48].

The individual spectra were then extinction corrected and co-added. Spectrophotometric standards taken from Oke (1974) and Oke & Gunn (1983) were used to flux calibrate the spectra. The goal was absolute spectrophotometry correct to within 10% and relative flux levels from the blue and red arms accurate enough to allow determination of the spectral indices. The flux calibration procedure was checked by flux-calibrating the standards and overlaying calibration points. It was found that calibration was reliable over the wavelength range 5500–8600 Å (ISIS red) and 3500–5500 Å (ISIS blue). Observations with a 5″ slit were obtained for all but three of the QSOs. These were reduced in the same way as the narrow-slit observations and used to correct the absolute flux levels for slit losses. The slit losses ranged from 0 to 50%.

"Featureless" B stars were selected from the Bright Star Catalogue (Hoffleit & Jaschek 1982) or Sky Catalogue 2000.0 (Hirshfeld, Sinnott, & Ochsenbien 1991) for use in removing the effects of atmospheric absorption in the red spectra (e.g., O_2 A band at 7600 Å). Observations of B stars were taken at different air masses to provide a range of absorption so that as many objects as possible could be

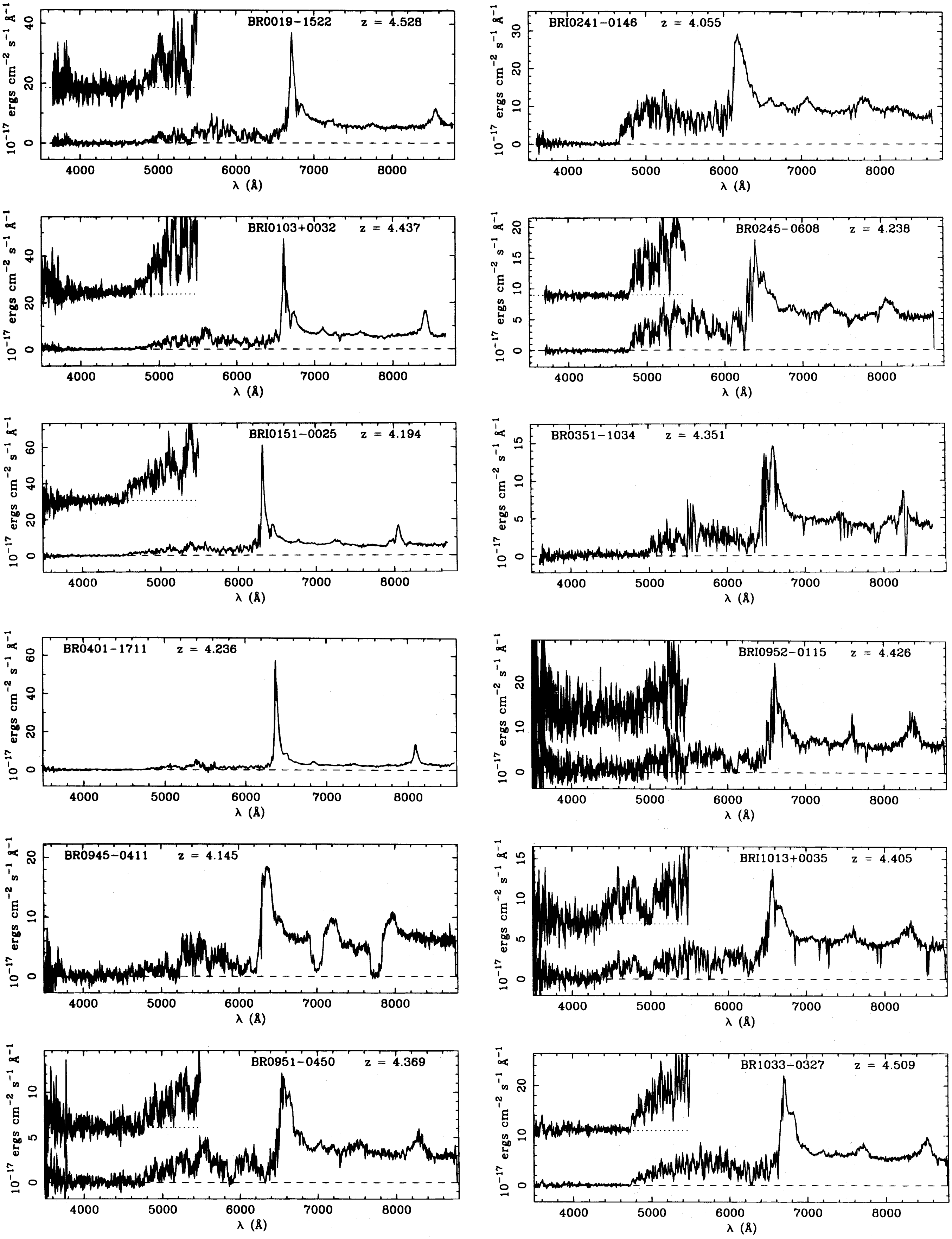

FIG. 4.—The final flux-calibrated spectra. The $z > 4.2$ QSOs used in the Lyman limit system evolution analysis show the region blueward of 5500 Å magnified in the upper left-hand corner. All except BR 0351−1034, BR 0401−1711 and BR 2237−0607 show the flux corrected for slit losses. BR 2248−1242 is shown twice. The second panel has the Lyα and C IV emission lines cut off to show the additional lines visible in the spectrum.

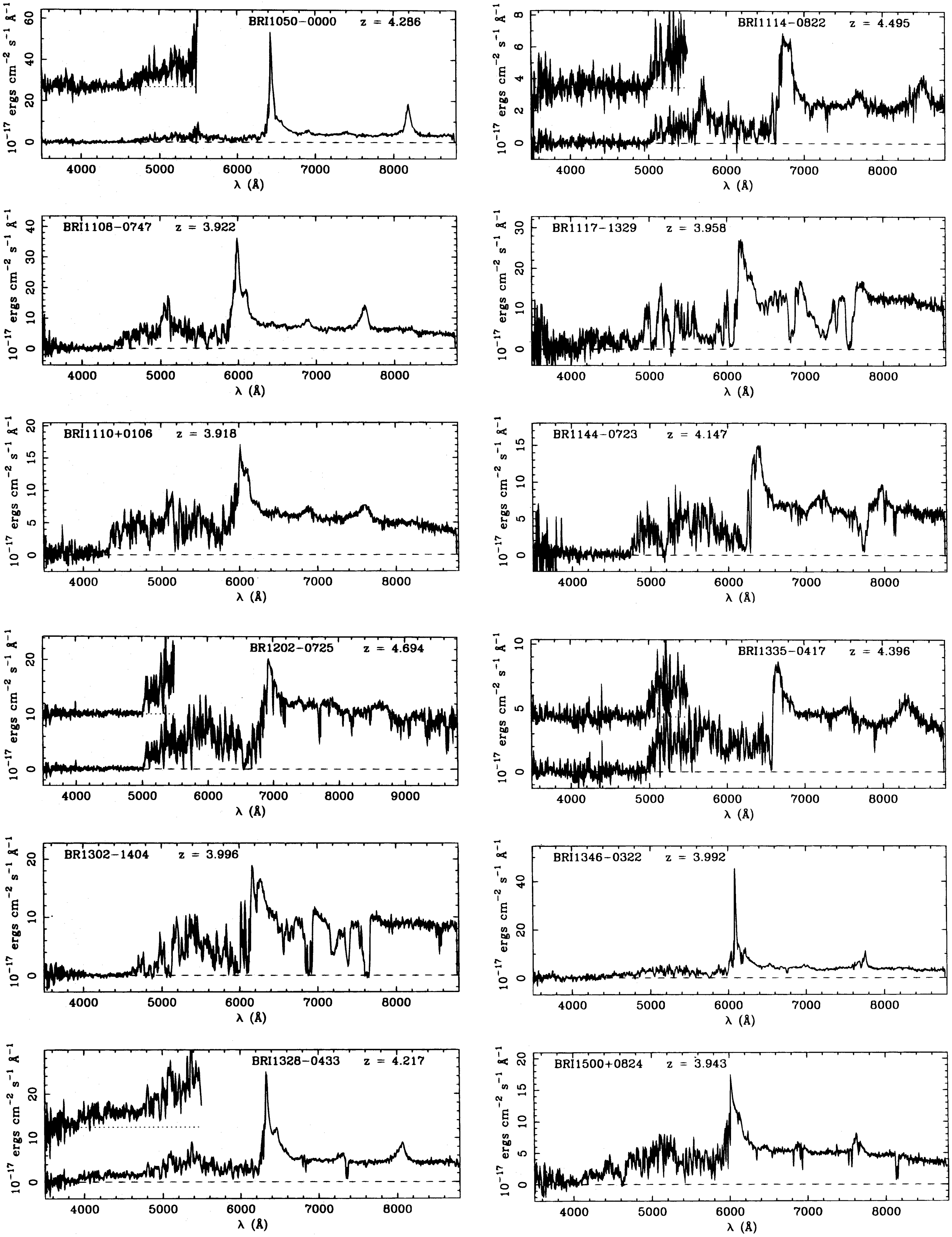

FIG. 4.—*Continued*

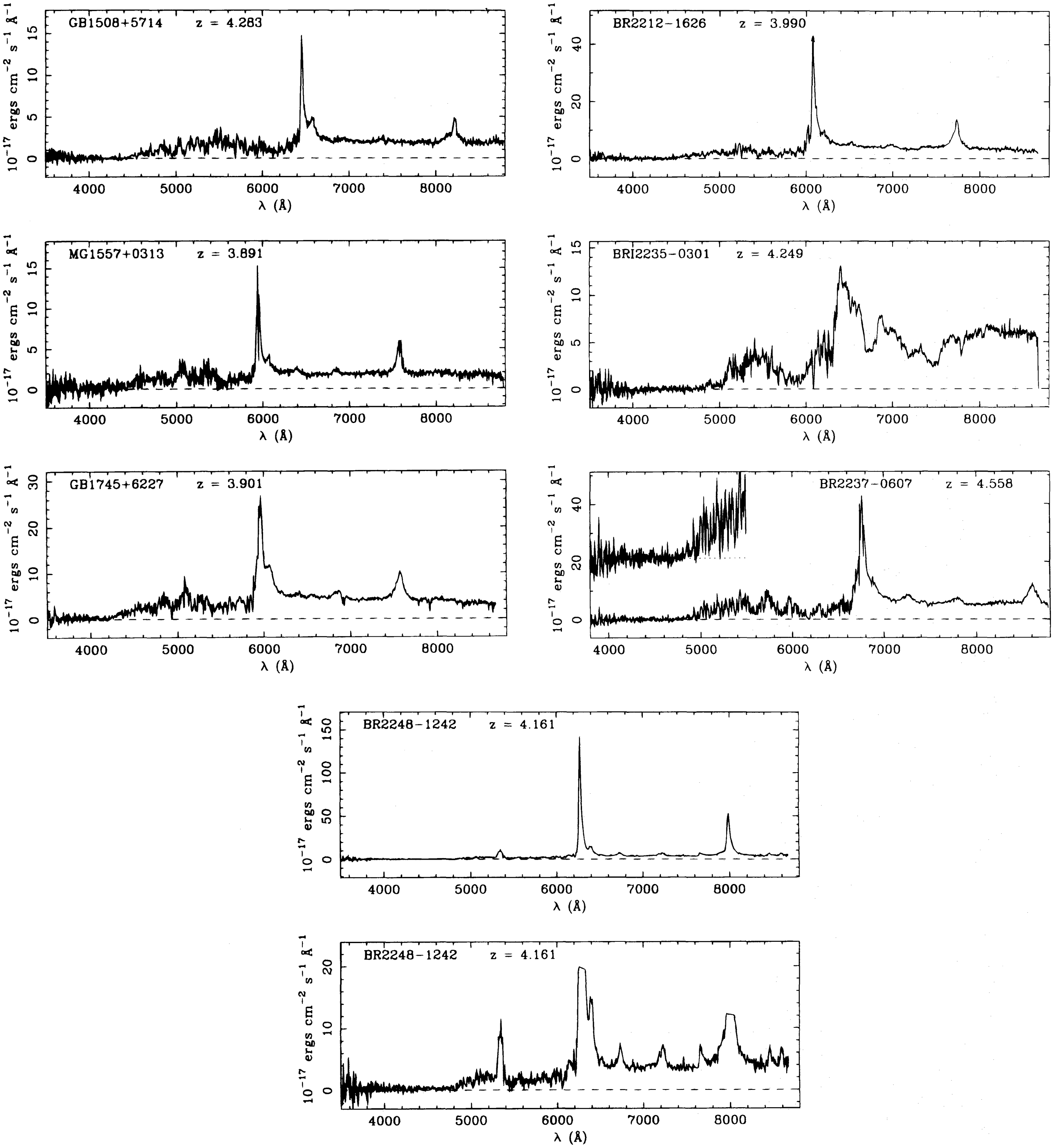

FIG. 4.—*Continued*

corrected. The spectrum of HR 4468 taken at an air mass of 1.48 is shown in Figure 2 and HD 13679 taken at an air mass of 1.06 is shown in Figure 3*a*. The atmospheric absorption features seen in the B-star spectrum were removed by interpolating between values on either side of the feature, resulting in the spectrum shown in Figure 3*b*. The original B-star spectrum was then divided by this featureless spectrum with the result shown in Figure 3*c*. The object spectra taken at comparable air masses were then divided by the result. The technique was successful in almost all cases, although it remains an art form to do it properly.

The red and blue arm spectra were joined using SCOMBINE. The final reduced spectra are shown in Figure 4, and the individual QSOs are described in § 5. The *AB* magnitude[3] measured at $\lambda_{\rm rest} = 1450$ Å and $\lambda_{\rm observed} = 7000$

---

[3] $AB = -2.5 * \log[f(\nu)$ (ergs s^{-1} cm^{-2} Hz^{-1})$] = -48.6$ as defined by Oke (1969).

TABLE 2

QSO MAGNITUDES AND POSITIONS

QSO	APM R	AB (7000 Å)	AB [1450 Å × (1 + z)]	B1950.0 R.A.	B1950.0 Declination	REFERENCES
BR 0019−1522	19.0	18.8	18.8	00 19 35.9	−15 22 17	1
BRI 0103+0032	18.6	18.9	18.8	01 03 45.2	+00 32 21	1
BRI 0151−0025	18.9	19.0	18.9	01 51 06.0	−00 25 49	1
BRI 0241−0146	18.2	18.4	18.4	02 41 29.3	−01 46 42	1
BR 0245−0608	18.6	18.9	18.8	02 45 27.4	−06 08 27	1
BR 0351−1034[a]	18.6	...	...	03 51 23.7	−10 34 08	1
BR 0401−1711[b]	18.7	...	...	04 01 40.8	−17 11 34	1
BR 0945−0411[c]	18.8	18.9	18.9	09 45 18.6	−04 11 17	1
BR 0951−0450	18.9	19.4	19.2	09 51 25.0	−04 50 07	1
BRI 0952−0115	18.7	18.8	18.7	09 52 27.2	−01 15 53	1
BRI 1013+0035	18.8	19.1	19.0	10 13 15.0	+00 35 17	1
BR 1033−0327	18.5	18.8	18.8	10 33 51.5	−03 27 46	1
BRI 1050−0000	18.6	19.5	19.4	10 50 46.7	−00 00 50	1
BRI 1108−0747	18.1	18.8	18.8	11 08 41.9	−07 47 44	1
BRI 1110+0106	18.3	19.0	18.9	11 10 12.3	+01 06 18	1
BRI 1114−0822	19.4	20.1	19.7	11 14 55.2	−08 22 34	1
BR 1117−1329[c]	18.0	18.1	18.1	11 17 39.4	−13 29 59	1
BR 1144−0723[c]	18.6	18.9	18.8	11 44 02.4	−07 23 25	1
BR 1202−0725	18.7	18.1	18.0	12 02 49.2	−07 25 50	1
BR 1302−1404[c]	18.6	18.4	18.4	13 02 46.8	−14 04 38	1
BRI 1328−0433	19.0	19.1	19.1	13 28 54.9	−04 33 26	1
BRI 1335−0417	19.4	19.2	19.1	13 35 27.5	−04 17 21	1
BRI 1346−0322	18.8	19.4	19.4	13 46 41.1	−03 22 22	1
BRI 1500+0824	19.3	19.1	19.1	15 00 18.6	+08 24 49	1
GB 1508+5714	18.9	20.0	19.8	15 08 45.2	+57 14 02	2
MG 1557+0313	19.8	20.0	20.0	15 57 00.5	+03 13 15	3
GB 1745+6227	18.3	19.3	19.3	17 45 48.0	+62 27 55	2
BR 2212−1626	18.1	18.7	18.6	22 12 44.8	−16 26 30	1
BRI 2235−0301[c]	18.2	18.5	18.5	22 35 47.4	−03 01 30	1
BR 2237−0607[a]	18.3	...	...	22 37 17.4	−06 07 59	1
BR 2248−1242	18.5	19.5	19.4	22 48 39.8	−12 42 59	1

NOTE.—The APM R magnitudes are measured from the APM scans of the UK Schmidt plates. The errors are estimated to be ± 0.25. The AB magnitudes at $\lambda = 7000$ Å and $\lambda = 1450$ Å × $(1 + z)$ are calculated from the flux measured in the wide slit observations listed in Table 1 using $AB = -2.5* \log [f(\nu)\ (\mathrm{ergs\ s^{-1}\ cm^{-2}\ Hz^{-1}})] = -48.6$ as defined by Oke 1969. The errors are estimated to be ± 0.1. The AB measures are 0.3 mag fainter at 7000 Å and from 0.3–0.5 mag fainter at 1450 Å × $(1 + z)$ than magnitudes measured with respect to Vega.

[a] No wide slit observations were obtained.

[b] Not photometric conditions.

[c] Exhibits broad absorption lines (BAL).

REFERENCES.—(1) Irwin et al. 1996; (2) Hook et al. 1995; (3) McMahon et al. 1996.

Å, along with the APM R magnitudes measured from the plate scans are listed in Table 2.

Using the absolute flux calibration for Vega taken from Hayes & Latham (1975) and defining the zero point of the AB magnitude system at $\lambda = 5556$ Å leads to the following magnitude zero-point differences: AB measures at $\lambda = 7000$ Å are 0.25 mag fainter than on a Vega-based system; for $\lambda = 1450 \times (1 + z)$ Å the difference ranges between 0.3 and 0.5 mag for a $4 \lesssim z \lesssim 5$ sample; the effective wavelength of the photographic R band is $\lambda = 6500$ Å, and the difference between the systems here is 0.2 mag. The 1 σ errors are ± 0.1. For those objects with no long-slit observations or nonphotometric conditions, only the APM R magnitude is quoted.

4. REDSHIFT MEASUREMENTS

4.1. *Measuring the Emission-Line Redshifts*

At redshifts greater than 4, Lyα + N V (rest wavelengths 1215.67 and 1240.13 Å) and C IV (1549.1 Å) are usually the only strong emission lines visible. Lyα is almost 50% absorbed by the Lyα forest, making it difficult to use for redshift determination. Emission lines from Lyβ (1025.72 Å), O VI (1034.0 Å), Si II (1263.0 Å), O I (1304.46 Å), C II (1335.0 Å), Si IV + O IV] (1400.0 Å), N IV] (1486.0 Å), He II (1640.4 Å), and O III] (1663.0 Å) may also be detected. Single Gaussians were fitted to the emission lines in each QSO, and the redshifts for each line were determined from the central wavelength ($z = \lambda_{\mathrm{observed}}/\lambda_{\mathrm{emitted}} - 1$). For the Ly$\alpha$ + N V blend the fit was mainly to the red wing due to the absorption by the forest. The redshifts for the strong metal lines were then averaged together (excluding Lyα) to determine a mean redshift for the QSO. The redshift of each of the emission lines, the mean QSO redshift, the 1 σ error, and the lines used in the determination are shown in Table 3.

4.2. *Emission-Line Velocity Shifts*

There are uncertainties in the systemic redshift of the QSOs in that redshifts determined from high- and low-ionization lines have been shown to exhibit velocity differences up to 2000 km s^{-1} (e.g., Espey et al. 1989; Steidel & Sargent 1991; Carswell et al. 1991; Tytler & Fan 1992), where the velocity difference, Δv, is defined as

$$\Delta v = c\,\frac{z_{\mathrm{ion}} - z_{\mathrm{C\,IV}}}{(1 + z_{\mathrm{C\,IV}})}\,.$$

TABLE 3

DETERMINATION OF QSO EMISSION REDSHIFTS

QSO	Redshift	Lyβ 1026 Å	O VI λ1034	Lyα 1216 Å	N V λ1240	Si II λ1263	O I λ1304	C II λ1335	Si/O IV λ1400	C IV λ1549	He II λ1640	O III] λ1663
BR 0019−1522	4.528 ± 0.005	…	…	4.531	…	…	**4.523**	…	**4.533**	**4.526**	…	…
BRI 0103+0032	4.437 ± 0.012	…	…	4.444	4.435	…	**4.447**	**4.447**	**4.422**	**4.430**	…	…
BRI 0151−0025	4.194 ± 0.009	…	…	4.218	4.205	…	**4.189**	**4.204**	**4.185**	**4.199**	…	…
BRI 0241−0146	4.053 ± 0.008	…	…	4.090	…	…	**4.058**	**4.060**	**4.052**	**4.042**	3.994	…
BR 0245−0608	4.238 ± 0.013	…	…	4.265	4.200	…	**4.250**	…	**4.240**	**4.223**	…	…
BR 0351−1034	4.351 ± 0.005[a]	…	…	4.398	4.320	…	…	…	4.327	4.327	…	…
BR 0401−1711	4.236 ± 0.014	4.261	…	4.251	4.257	…	**4.247**	…	**4.235**	**4.227**	…	…
BR 0945−0411	4.145 ± 0.010	…	…	4.174	4.147	…	…	…	4.146	**4.145**	…	…
BR 0951−0450	4.369 ± 0.022	…	…	4.433	4.438	**4.339**	**4.390**	**4.386**	**4.377**	**4.345**	4.336	…
BRI 0952−0115	4.426 ± 0.020	…	…	4.467	…	…	**4.448**	**4.432**	**4.425**	**4.400**	…	…
BRI 1013+0035	4.405 ± 0.038	…	…	4.442	…	…	…	…	**4.432**	**4.378**	…	…
BR 1033−0327	4.509 ± 0.005	…	…	4.521	4.503	…	**4.511**	**4.516**	**4.507**	**4.504**	…	…
BRI 1050−0000	4.286 ± 0.005	…	4.310	4.294	…	…	**4.291**	…	**4.281**	**4.285**	…	…
BRI 1108−0747	3.922 ± 0.008	3.924	3.932	3.936	3.919	…	**3.934**	**3.921**	**3.917**	**3.915**	…	3.926
BRI 1110+0106	3.918 ± 0.006	…	…	3.988	…	…	…	…	**3.916**	**3.913**	**3.924**	…
BRI 1114−0822	4.495 ± 0.004	4.518	4.516	4.557	…	…	4.455	**4.491**	**4.498**	**4.497**	…	…
BR 1117−1329	3.958 ± 0.031	3.983	3.982	4.043	…	…	**3.925**	…	**3.964**	**3.986**	…	…
BR 1144−0723	4.147 ± 0.004	…	…	4.169	4.152	…	…	…	**4.145**	**4.150**	…	…
BR 1202−0725	4.694 ± 0.010[b]	…	…	**4.694**	…	…	…	…	…	4.679	…	…
BR 1302−1404	3.996 ± 0.013	…	…	4.078	4.060	…	…	…	**3.986**	**4.005**	…	…
BRI 1328−0433	4.217 ± 0.011	…	…	4.224	4.181	…	**4.223**	…	**4.223**	**4.205**	…	…
BRI 1335−0417	4.396 ± 0.026	…	…	4.489	4.381	…	**4.410**	**4.426**	**4.378**	**4.370**	…	…
BRI 1346−0322	3.992 ± 0.014	…	…	4.011	3.984	…	**4.004**	…	**3.976**	**3.996**	3.935	3.965
BRI 1500+0824	3.943 ± 0.013	…	…	3.991	…	…	**3.950**	…	**3.951**	**3.928**	…	…
GB 1508+5714	4.283 ± 0.019	…	…	4.309	4.292	…	**4.266**	…	**4.279**	**4.304**	…	…
MG 1557+0313	3.891 ± 0.001	…	3.900	3.896	3.845	…	**3.889**	…	**3.892**	**3.891**	…	…
GB 1745+6227	3.901 ± 0.016	…	3.903	3.910	3.876	…	**3.911**	**3.919**	**3.888**	**3.888**	…	…
BR 2212−1626	3.990 ± 0.002	…	…	4.005	3.952	…	**3.990**	…	**3.988**	**3.992**	…	…
BRI 2235−0301	4.249 ± 0.018	…	…	4.322	…	…	**4.269**	**4.245**	…	**4.234**	…	…
BR 2237−0607	4.558 ± 0.003	…	…	4.569	…	…	**4.559**	…	**4.562**	**4.555**	…	…
BR 2248−1242	4.161 ± 0.002	…	4.168	4.164	4.111	4.160	**4.163**	4.165	**4.159**	**4.160**	4.160	4.168

NOTE.—The redshifts in boldface type were used to calculate the mean QSO emission redshift.

[a] Redshift calculated from the strong C IV absorption doublet.

[b] Redshift calculated from the Lyα edge. The redshift quoted for C IV in the table is for an absorption feature.

TABLE 4

EMISSION-LINE VELOCITY SHIFTS

Line Pair	Median[a,c] Δv (km s^{-1})	Mean[a] Δv (km s^{-1})	σ (km s^{-1})	N[b]
Lyβ–C IV	850 ± 210	850	420	2
O VI– C IV	1040 ± 50	930	330	7
Lyα–C IV	1100 ± 70	2050	1790	25
N V–C IV...............	−680 ± 130	−450	1930	15
Si II–C IV...............	−170 ± 120	−170	240	2
O I–C IV	430 ± 60	550	1260	22
C II– C IV	940 ± 100	1130	1040	11
Si IV+O IV]–C IV......	140 ± 40	320	960	24
He II–C IV	−500 ± 376	−1270	1880	5
O III]–C IV.............	470 ± 470	−240	1410	3

NOTE.—The emission-line redshifts are listed in Table 3.

[a] $\Delta v = c*(z - z_{\mathrm{C\,IV}})/(1 + z_{\mathrm{C\,IV}})$

[b] N denotes the number of pairs of lines used in the calculation

[c] The error is σ/N.

The same trend is exhibited in the APM sample, with a median difference of 430 ± 60 km s^{-1} between O I and C IV, with the high-ionization line C IV blueshifted with respect to the O I. The velocity difference relative to C IV has been calculated for all the measured emission lines, and the results are summarized in Table 4.

The BAL QSOs have been excluded from this analysis. Histograms of the velocity differences are shown in Figure 5. Some of the very large differences of several thousand kilometers per second are due to the difficulty in accurately measuring some of the heavily absorbed emission lines, e.g., Lyα. These shifts are important in estimating the metagalactic ultraviolet background flux based on the proximity effect (e.g., Williger et al. 1994), since an error in the redshift of the QSO of ~1000 km s^{-1} can lead to a factor of 2–3 error in the derived ionizing flux.

5. EMISSION AND ABSORPTION FEATURES

The character of the emission lines and the H I and metal absorption systems detected are described below for each QSO. Additional analysis of the intrinsic properties of the QSOs are described in a separate paper (Storrie-Lombardi et al. 1997). The metal absorption systems in the non-BAL QSOs were selected with an automated algorithm that detected absorption features redward of Lyα emission with an equivalent width $W \geq 3\,\sigma$ in 2.5 resolution elements. In the cases where the feature detected included more than one line, Gaussians were fitted to the lines individually to measure the redshifts and equivalent widths. The results, with 1 σ errors, are listed in Table 5, along with the identification of ion and redshift where possible. The selection of the damped Lyα candidates is discussed in § 6, and the Lyman limit systems previously published in Storrie-Lombardi et al. (1994) are summarized in Table 6.

5.1. *BR 0019−1522* ($z_{\mathrm{em}} = 4.528$)

The Lyα + N V and C IV emission lines are strong and sharp. There is a Lyman-limit system at $z = 4.27$ and a damped Lyα candidate system at $z = 3.98$. Si II, C IV, and Fe II absorption are observed at $z = 3.4$.

5.2. *BRI 0103+0032* ($z_{\mathrm{em}} = 4.437$)

Strong and sharp Lyα and C IV, with weaker O I, C II, and Si IV + O IV] can be seen. There is weak Mg II at $z = 1.818$

TABLE 5

METAL ABSORPTION SYSTEMS

QSO	λ (Å)	W	σ (W)	Ion	z
BR 0019−1522.......	6777.7	4.4	0.3	Si II	3.439
	6805.5	5.0	0.4	C IV	3.396
	6819.3	1.7	0.4	C IV	3.396
	7141.0	2.0	0.5	Fe II	3.440
	7153.9	1.9	0.4	...	...
	7417.2	3.4	0.5	...	...
BRI 0103+0032......	6616.6	3.4	0.1	Mg II	1.366
	6634.2	5.4	0.2	Mg II	1.366
	6664.6	1.0	0.2	...	...
	6695.1	9.7	0.4	Fe II	1.810
	7325.0	8.3	0.7	Fe II	1.817
	7880.5	2.2	0.6	Mg II	1.818
	7898.5	4.2	0.7	Mg II	1.818
BRI 0151−0025......	6405.0	5.9	0.4	N V	4.170
	6425.0	4.3	0.3	N V	4.170
	7549.7	1.1	0.3	C IV	3.876
	7562.7	1.0	0.3	C IV or Fe II	3.876 1.908
	7582.9	2.9	0.6	...	...
	7890.0	1.2	0.3	...	...
	8003.1	6.2	0.7	Fe II	1.910
	8132.4	4.7	0.8	Mg II	1.908
	8153.5	4.4	0.8	Mg II	1.908
	8628.2	3.8	1.2	...	...
BRI 0241−0146......	6317.8	1.1	0.4	...	...
	6336.9	1.7	0.5	Fe II	1.437
	6382.3	1.4	0.4	...	...
	6467.4	1.5	0.5	...	...
	6809.0	0.6	0.2	Mg II	1.435
	6827.8	0.7	0.2	Mg II	1.435
	6882.3	2.1	0.5	...	...
	6923.6	2.5	0.5	...	...
	6966.7	2.2	0.6	...	...
	7691.1	4.8	0.6	...	...
	8060.4	3.3	0.9	...	...
BR 0245−0608.......	6312.4	11.2	0.5	...	...
	6356.4	17.0	0.5	Fe II	1.712
	6380.5	4.9	0.4	...	...
	6438.0	4.6	0.4	Fe II	1.708
	6453.2	4.2	0.4	Fe II	1.712
	6477.5	0.9	0.2	C IV	3.184
	6488.0	3.2	0.4	C IV	3.184
	6861.5	2.8	0.6	...	...
	7047.2	1.9	0.5	Fe II	1.710
	7093.1	4.1	0.5	...	...
	7104.8	1.9	0.4	...	...
	7160.7	2.1	0.4	Si IV	4.139
	7208.3	3.0	0.5	Si IV	4.139
	7580.5	3.0	0.5	Mg II	1.711
	7600.9	3.5	0.6	Mg II	1.711
	7957.1	5.9	0.7	C IV	4.140
	7971.9	1.8	0.5	C IV	4.140
BR 0351−1034.......	6545.9	9.2	0.4	Mg II	1.340
	6559.5	7.9	0.4	Mg II	1.340
	6576.0	3.6	0.4	...	...
	6631.7	4.9	0.3	N V	4.353
	6653.0	4.4	0.4	N V	4.353
	6744.9	1.3	0.3	Si II	4.351
	6867.2	2.6	0.5	...	...
	6873.9	2.3	0.5	...	...
	6989.2	5.8	0.5	Fe II	1.933
	7000.7	3.5	0.4	...	...
	7105.2	1.4	0.4	Si IV	4.098
	7148.3	1.4	0.4	Si IV	4.098
	7173.5	2.0	0.6	C IV	3.633
	7185.2	1.2	0.5	C IV	3.633
	7196.0	0.7	0.2	...	...
	7431.7	1.5	0.4	...	...
	7458.8	6.6	0.5	Si IV	4.352
	7507.5	5.2	0.4	Si IV	4.352
	7550.7	5.0	0.6	...	...
	7822.5	3.3	0.5	...	...

TABLE 5—*Continued*

QSO	λ (Å)	W	σ (W)	Ion	z
	7834.6	2.4	0.5	…	…
	7843.6	2.0	0.5	…	…
	7895.7	12.6	0.7	C IV	4.098
	7906.9	11.4	0.7	C IV	4.098
	7916.4	8.5	0.5	…	…
	7940.0	11.1	0.7	…	…
	7952.2	8.4	0.5	…	…
	8159.8	6.0	0.5	…	…
	8173.1	4.7	0.5	…	…
	8188.0	3.7	0.5	…	…
	8197.0	3.4	0.5	Mg II	1.931
	8218.2	2.0	0.4	Mg II	1.931
	8228.1	2.4	0.4	C IV	4.315
	8241.9	2.2	0.4	C IV	4.315
	8286.8	21.5	1.0	C IV	4.351
	8297.7	15.1	1.0	C IV	4.351
BR 0401−1711.......	6382.5	2.7	0.1	…	…
	6972.7	1.6	0.3	…	…
	7198.9	3.1	0.3	…	…
	7297.7	2.4	0.3	…	…
	7307.9	2.2	0.3	…	…
	7344.4	1.6	0.3	…	…
	8095.0	2.7	0.1	C IV	4.229
	8109.5	2.0	0.1	C IV	4.229
	8396.9	4.9	0.8	…	…
BR 0951−0450.......	6553.5	5.7	0.4	Si IV	3.703
	6598.8	2.0	0.4	Si IV	3.703
	6614.1	3.1	0.4	…	…
	6712.6	4.2	0.6	…	…
	6769.5	3.5	0.6	Si IV	3.858
	6815.9	2.0	0.4	Si IV	3.858
	7282.7	5.5	0.7	C IV	3.703
	7293.3	4.2	0.7	C IV	3.703
	7359.6	5.0	1.1	…	…
	7416.0	3.3	0.6	Si II	3.858
	7456.7	2.4	0.7	…	…
	7517.4	2.1	0.6	C IV	3.855
	7528.4	2.8	0.6	C IV	3.855
	8108.8	7.1	1.1	…	…
	8306.1	1.8	0.5	C IV	4.364
	8317.3	1.1	0.3	C IV	4.364
BRI 0952−0115......	6648.4	2.0	0.2	C IV	3.294
	6660.2	1.3	0.2	C IV	3.294
	6704.9	6.3	0.4	C II	4.024
	6719.7	8.1	0.3	…	…
	6749.6	1.2	0.3	…	…
	6826.4	1.8	0.4	…	…
	6875.6	2.7	0.3	…	…
	6928.4	2.8	0.5	C IV	3.475
	6941.3	1.7	0.5	C IV	3.475
	7002.6	2.8	0.4	Si IV	4.024
	7047.6	2.2	0.4	Si IV	4.024
	7132.2	1.2	0.3	Fe II	1.993
	7208.8	2.4	0.5	…	…
	7306.4	4.6	0.5	C IV	3.719
	7317.6	3.6	0.5	C IV	3.719
	7345.5	1.6	0.5	…	…
	7478.4	1.6	0.5	…	…
	7669.4	3.9	0.5	Si II	4.024
	7776.9	7.9	0.6	C IV	4.023
	7788.5	3.2	0.6	C IV	4.023
	7987.2	3.3	0.8	…	…
	8082.3	1.9	0.5	Fe II	4.025
	8234.5	1.8	0.4	…	…
	8344.7	5.6	0.6	…	…
	8383.8	4.7	0.5	Mg II	1.993
	8403.9	2.5	0.4	Mg II	1.993
	8418.9	2.4	0.6	…	…
	8482.8	2.3	0.5	…	…
	8663.2	2.7	0.9	…	…
BRI 1013+0035......	6599.4	4.4	0.4	Fe II	3.103
	6855.6	6.3	0.5	…	…
	6911.3	2.5	0.5	Fe II	2.057
	7169.2	5.2	0.5	Fe II	2.059
	7260.8	3.3	0.6	Fe II	2.058
	7287.1	6.9	0.5	Fe II	2.058
	7303.2	0.8	0.2	…	…
	7324.8	3.0	0.7	…	…
	7907.7	5.2	0.9	Fe II	2.057
	7948.5	6.8	0.7	Fe II	2.057
	8539.9	8.4	0.6	Mg II	2.054
	8561.2	9.1	0.6	Mg II	2.054
BR 1033−0327.......	6689.2	2.9	0.2	…	…
	6869.4	1.9	0.3	C II	4.148
BRI 1050−0000......	6487.3	1.7	0.3	C II	3.861
	6776.0	2.1	0.5	Si IV	3.862
	6818.6	1.7	0.5	Si IV	3.862
	7528.0	3.7	0.6	C IV	3.862
	7538.1	4.3	0.6	C IV	3.862
	8117.7	1.6	0.3	…	…
	8141.8	0.6	0.2	…	…
BRI 1108−0747......	5977.9	6.1	0.3	…	…
	6630.1	2.6	0.5	…	…
	6791.7	3.1	0.4	…	…
	6804.1	0.7	0.2	…	…
	7083.9	1.4	0.4	C IV	3.575
	7094.0	1.1	0.3	C IV	3.575
	7132.3	2.5	0.4	C IV	3.607
	7143.8	1.2	0.4	C IV	3.607
	8310.5	4.2	0.9	…	…
BRI 1110+0106......	6413.0	2.7	0.5	Fe II	1.479
	6446.4	1.9	0.5	Fe II	1.479
	6634.7	1.4	0.4	…	…
	6932.2	1.6	0.4	Mg II	1.479
	6950.7	1.5	0.4	Mg II	1.479
	7158.6	1.7	0.5	…	…
	7299.6	1.6	0.5	…	…
	7323.0	2.4	0.6	…	…
	7829.7	2.2	0.7	Mg II	1.800
	7852.1	2.5	0.8	Mg II	1.800
	8574.3	4.5	1.1	…	…
BRI 1114−0723......	6697.5	3.0	0.3	Mg II	1.395
	6713.7	3.1	0.3	Mg II	1.395
	6846.4	1.6	0.3	C IV	3.422
	6858.7	1.2	0.3	C IV	3.422
	6877.1	4.8	0.6	…	…
	7016.4	2.5	0.6	…	…
	7076.9	3.6	0.4	C IV	3.571
	7088.1	1.9	0.4	C IV	3.571
	7105.2	2.0	0.4	C IV	3.589
	7116.3	1.4	0.3	C IV	3.589
	7280.2	4.3	0.5	…	…
	7300.6	3.6	0.4	…	…
	7329.1	1.7	0.4	…	…
	7812.8	2.8	0.4	Mg II	1.794
	7832.3	2.7	0.4	Mg II	1.794
	8331.5	4.2	1.3	…	…
BR 1202−0725.......	6888.5	5.6	0.3	Mg II	1.463
	6906.2	6.1	0.3	Mg II	1.463
	7005.0	3.8	0.3	C IV	3.525
	7017.2	1.3	0.3	C IV	3.525
	7067.4	1.4	0.3	C IV	3.565
	7079.9	0.8	0.2	C IV	3.565
	7122.3	2.8	0.3	Fe II	1.753
	7161.1	3.1	0.3	Fe II	1.754
	7183.2	3.8	0.2	C II	4.383
	7702.6	6.4	0.5	Mg II	1.754
	7722.2	4.4	0.4	Mg II	1.754
	7852.4	2.6	0.4	C IV	4.072
	7865.5	1.8	0.4	C IV	4.072
	8064.6	2.1	0.4	Fe II	2.441
	8194.9	7.6	0.6	Fe II	2.439
	8212.6	3.1	0.6	Si II	4.379
	8475.6	3.3	0.5	C IV	4.474

TABLE 5—*Continued*

QSO	λ (Å)	W	σ (W)	Ion	z
	8491.3	1.8	0.4	C IV	4.474
	8793.0	3.8	0.5	C IV	4.679
	8806.1	1.4	0.4	C IV	4.679
	8891.4	2.5	0.6	Fe II	2.437
	8937.7	2.7	0.7	Fe II	2.438
	9053.9	3.9	0.9	Mg II	2.238
	9076.2	3.1	0.7	Mg II	2.238
	9314.7	4.6	0.6	…	…
	9337.1	8.4	0.6	Mg II	2.339
	9360.1	5.8	0.6	Mg II	2.339
	9526.4	4.5	1.3	Mg I	2.339
	9630.6	13.4	1.0	Mg II	2.444
	9656.1	9.8	1.0	Mg II	2.444
BRI 1328−0433……	6797.6	5.4	0.5	Fe II	1.628
	6832.7	8.0	0.7	Fe II	1.628
	6862.8	2.9	0.6	…	…
	7349.4	15.0	0.6	Mg II	1.628
	7367.6	13.2	0.6	Mg II	1.628
BRI 1335−0417……	6617.0	2.4	0.3	Fe II	1.823
	6702.4	1.3	0.4	Fe II	1.823
	6725.3	3.3	0.5	Fe II	1.822
	6813.9	2.9	0.6	Si II	4.406
	7210.6	3.3	0.8	C II	4.403
	7339.6	2.4	0.6	Fe II	1.823
	7696.9	2.6	0.5	…	…
	7707.6	5.2	0.5	…	…
	7892.6	5.5	0.7	Mg II	1.822
	7914.8	4.4	1.1	Mg II	1.822
BRI 1346−0322……	6115.7	1.6	0.2	…	…
	6160.4	6.3	0.4	N V	3.974
	6182.3	7.4	0.4	N V	3.974
	6207.1	1.1	0.3	…	…
	6428.4	1.8	0.6	…	…
	6654.7	1.8	0.6	Fe II	1.943
	6749.8	7.5	0.8	C IV	3.359
	6760.2	5.0	0.7	C IV	3.359
	6986.5	1.2	0.3	Fe II	1.943
	7002.2	1.8	0.5	Si IV	3.992
	7705.7	9.9	0.7	C IV	3.974
	7737.3	4.1	0.5	C IV	3.994
	8116.9	3.0	0.8	C IV	3.994
	8222.1	1.2	0.8	…	…
	8231.8	1.8	0.8	Mg II	1.944
BRI 1500+0824……	6106.8	1.4	0.3	Fe II	2.797
	6343.9	4.0	0.5	Al II	2.796
	6545.6	1.7	0.5	…	…
	6819.0	4.9	0.7	Fe II	1.909
	6907.6	4.0	0.4	Fe II	1.910
	6931.3	7.3	0.6	Fe II	1.909
	7524.2	3.9	0.6	Fe II	1.908
	7563.7	7.7	0.8	Fe II	1.909
	7648.5	2.4	0.4	C IV	3.940
	7660.8	2.8	0.4	C IV	3.940
	8130.5	14.8	0.7	Mg II	1.908
	8150.1	10.6	0.7	Mg II	1.908
GB1508+5714 …….	6518.1	2.3	0.5	…	…
	7428.5	3.7	1.1	…	…
MG 1557+0313……	5952.6	6.4	0.3	…	…
	7583.3	2.4	0.4	C IV	3.898
	7596.1	1.5	0.4	C IV	3.898
GB 1745+6227 ……	5957.5	1.8	0.2	…	…
	6910.1	6.2	0.7	Mg II	1.471
	6928.8	6.3	0.7	Mg II	1.471
	7098.1	2.0	0.6	…	…
	7512.3	1.3	0.4	Fe II	2.323
	7785.8	3.2	0.8	Fe II	2.322
	7887.3	2.7	0.8	Fe II	2.322
	7914.9	6.9	1.1	Fe II	2.321
	8590.3	4.1	1.1	Fe II	2.321
	8637.0	6.1	1.3	Fe II	2.322
BR 2212−1626…….	6167.3	2.8	0.6	…	…
	6276.0	2.3	0.5	…	…

TABLE 5—*Continued*

QSO	λ (Å)	W	σ (W)	Ion	z
	6496.3	2.1	0.6	…	…
	8236.0	2.5	0.8	…	…
BR 2237−0607……	6777.2	2.8	0.1	C II	4.078
	6868.8	1.7	0.4	N V	4.545
	6888.0	1.1	0.2	N V	4.545
	7079.1	2.2	0.5	Si IV	4.079
	7126.9	1.7	0.5	Si IV or Fe II	4.079 2.152
	7310.2	1.6	0.6	…	…
	7385.6	1.4	0.4	Fe II	2.151
	7472.4	3.6	0.5	Mg II	1.672
	7491.4	1.1	0.3	Mg II or Fe II	1.672 2.156
	7519.2	1.5	0.5	Fe II	2.155
	8164.1	1.6	0.5	Fe II	2.156
	8487.7	1.6	0.5	C IV	4.482
	8502.3	0.6	0.2	C IV	4.482
BR 2248−1242……	6487.5	6.0	1.1	…	…
	7202.4	2.2	0.6	…	…
	7939.5	2.0	0.6	…	…

with two corresponding Fe II lines and Mg II at $z = 1.366$. There are absorption edges visible just shortward of the emission lines that correspond to O I + Si II at $z = 4.41$ and Si IV and C IV at $z = 4.37$. There are two Lyman-limit systems at $z = 4.31$ and 4.15.

5.3. *BRI 0151−0025* ($z_{\mathrm{em}} = 4.194$)

The Lyα and C IV emission lines are strong and sharp with weaker O I and Si IV + O IV] emission. There is a Lyman-limit system at $z = 4.05$ and C IV at $z = 3.876$. At $z = 4.17$ there is a strong Lyα absorption line, a N V

TABLE 6

APM COLOR SURVEY LYMAN-LIMIT SYSTEMS

QSO[a]	z_{em}	z_{min}	z_{LLS}	τ_{LLS}
BR 0019−1522……..	4.52	2.51	4.27	>5.8
BRI 0103+0032…….	4.44	2.51	4.31	1.6
	…	…	4.15	>1.6
BRI 0151−0025…….	4.20	2.51	4.05	>3.7
BR 0245−0608……..	4.24	2.51	4.23	>3.9
BR 0951−0450……..	4.37	2.84	4.22	>3.1
BRI 0952−0115…….	4.43	2.84	4.25	>2.1
BRI 1013+0035…….	4.41	2.84	3.78	>2.3
BR 1033−0327……..	4.51	2.84	4.19	>3.5
BRI 1050−0000…….	4.29	2.84	4.08	>2.5
BRI 1114−0822[b]……	4.51	2.84	4.50	>3.7
BR 1202−0725……..	4.69	2.84	4.52	>3.0
BRI 1328−0433…….	4.22	2.84	4.25	0.6
	…	…	3.31	>1.5
BRI 1335−0417[b]……	4.40	2.84	4.45	>3.1
GB 1508+5714 …….	4.30	2.84	3.88	>4.6
BR 2237−0607……..	4.56	2.51	4.28	>2.6

NOTE.—z_{em} = QSO emission redshift; z_{min} = minimum z at which a LLS could be observed; z_{LLS} = Lyman-limit system redshift; τ_{LLS} = optical depth at the Lyman limit.

[a] $z_{\mathrm{em}} \geq 4.2$, used in Storrie-Lombardi et al. 1994.

[b] $[(z_{\mathrm{em}} - z_{\mathrm{LLS}})/(1+z_{\mathrm{em}})] \times c < 4000\ \mathrm{km\ s^{-1}}$.

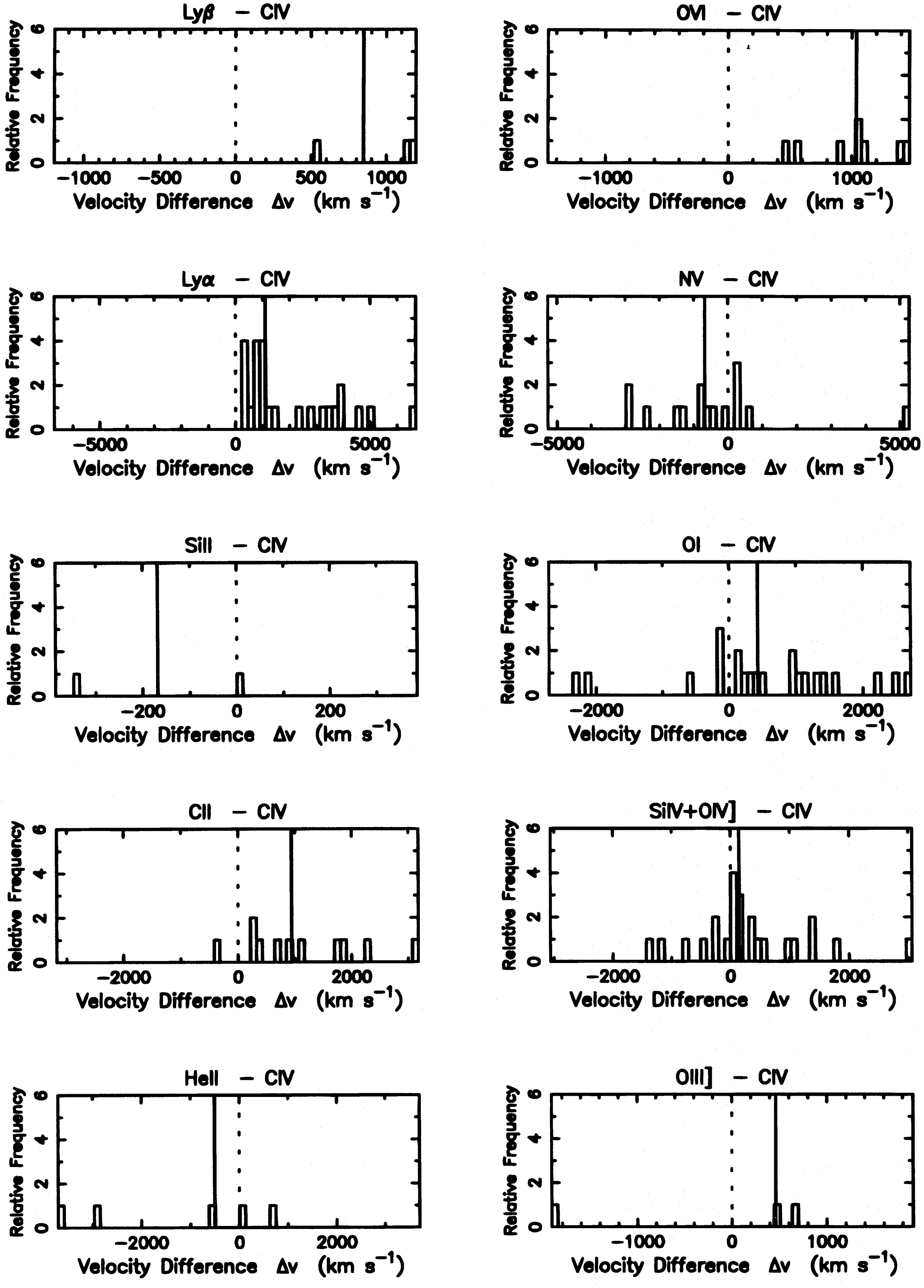

FIG. 5.—Histograms of the velocity difference relative to C IV for all the measured emission lines are shown. These are tabulated in Table 4. Some of the very large differences of several thousand kilometers per second are due to the difficulty in accurately measuring some of the heavily absorbed emission lines, e.g. Lyα.

doublet, and a single line that could be C IV. There is Mg II with at least one Fe II line at $z = 1.91$.

5.4. *BRI 0241−0146* ($z_{\rm em} = 4.053$)

The Lyα + N V, O I, C II, Si IV + O IV], and C IV emission lines are broad and rounded. There is a strong Lyman-limit system at $z = 4.10$. There are numerous absorption lines redward of the Lyα emission, but they are not easily identifiable. Mg II and Fe II are identified at $z = 1.435$. Shallow absorption troughs are also visible.

5.5. *BR 0245−0608* ($z_{\rm em} = 4.238$)

The Lyα + N V, O I, Si IV + O IV], and C IV emission lines are weak. There is strong Lyα absorption on the blue side of the Lyα emission corresponding to the Lyman-limit system at $z = 4.23$. An Mg II doublet with four corresponding Fe II lines is observed at $z = 1.711$. There are strong, narrow Lyα absorption lines (although not damped candidates) at $z = 3.36$ and 4.14, with corresponding Si IV and C IV at $z = 4.14$. C IV is also detected at $z = 3.184$.

5.6. *BR 0351−1034* ($z_{\rm em} = 4.351$)

This is one of the most unusual objects in the survey, with saturated C IV absorption in the middle of the C IV emission. There are a large number of absorption lines, including Si IV at $z = 4.098$ and 4.352, C IV at $z = 3.633$, 4.098, 4.351, and 4.351, Mg II at $z = 1.340$ and 1.931, and N V at $z = 4.353$. Due to the difficulty in measuring redshifts from the heavily absorbed emission lines, the redshift for this object was calculated from the C IV absorption at $z = 4.351$.

5.7. *BR 0401−1711* ($z_{\rm em} = 4.236$)

The Lyα + N V, O I, and C IV emission lines are strong and sharp, while the Si IV + O IV] is broader and weaker. The O I is unusually prominent. There is strong absorption in the C IV emission line at $z = 4.229$. There is Lyman limit system at the QSO redshift. The absorption feature at $\sim$7600 Å is a residual from the removal of the atmospheric absorption line. The spectrum is very noisy at the red end of the blue arm portion ($\sim$5600 Å) and does not join together smoothly with the red arm spectrum.

5.8. *BR 0945−0411* ($z_{\rm em} = 4.145$, BAL)

This is the first of the five QSOs in the APM Color Survey that exhibits broad absorption lines. O VI, N V, Si IV, and C IV are observed at $z \approx 4.01$.

5.9. *BR 0951−0450* ($z_{\rm em} = 4.369$)

The Lyα + N V, O I, C II, Si IV + O IV], and C IV emission lines are weak. There are damped Lyα candidates at $z = 3.84$ and 4.20. C IV doublets are identified at $z = 3.703$, 3.855, 4.196, and 4.364 and Si IV at $z = 3.703$ and 3.858. There is a Lyman-limit system at $z = 4.22$.

5.10. *BRI 0952−0115* ($z_{\rm em} = 4.426$)

This QSO is gravitationally lensed (McMahon, Irwin, & Hazard 1992). The Lyα + N V, Si IV + O IV], and C IV emission are weak and heavily absorbed. There is a strong damped Lyα candidate at $z = 4.01$. C IV doublets are identified at $z = 3.294$, 3.475, 3.719, and 4.023 and Mg II at $z = 1.993$. There is a Lyman-limit system at $z = 4.25$.

5.11. *BRI 1013+0035* ($z_{\rm em} = 4.405$)

The Lyα + N V, O I, C II, Si IV + O IV], and C IV emission lines are weak. There is a damped Lyα candidate at $z = 3.10$ with corresponding Fe II detected. There is an Mg II doublet at $z = 2.054$ with six corresponding Fe II lines at $z = 2.058$. There is a Lyman-limit system at $z = 3.78$.

5.12. *BR 1033−0327* ($z_{\rm em} = 4.509$)

The Lyα + N V, O I, C II, Si V + O IV], and C IV emission lines fall at the strong end of the weaker lined objects. There is a Lyman-limit system at $z = 4.19$ and C II tentatively identified at $z = 4.148$. See Williger et al. (1994) for a detailed analysis of the Lyα forest region in this object.

5.13. *BRI 1050−0000* ($z_{\rm em} = 4.286$)

The Lyα and C IV emission lines are strong and sharp with weaker O VI, O I, and Si IV + O IV] emission. There is C II, Si IV, and C IV detected at $z = 3.862$ and a Lyman-limit system at $z = 4.08$.

5.14. *BRI 1108−0747* ($z_{\rm em} = 3.922$)

The Lyα and C IV emission are strong, and this is one of the few objects where Lyβ, O VI, and N V are easily distinguished, along with O I, C II, Si IV + O IV], and N IV]. C IV doublets are observed at $z = 3.575$, and 3.607.

5.15. *BRI 1110+0106* ($z_{\rm em} = 3.918$)

The Lyα + N V, O I, C II, Si IV + O IV], and C IV emission are weak. The O_2 A-band atmospheric absorption has been removed from the C IV emission line, and a residual spike was cut off, resulting in the unreal flat top to the emission line. Mg II and two Fe II lines are observed at $z = 1.479$ and Mg II at $z = 1.800$.

5.16. *BRI 1114−0822* ($z_{\rm em} = 4.495$)

The Lyα + N V, Si IV + O IV], and C IV emission lines are weak, although the Lyβ + O VI is fairly prominent. There is a damped Lyα candidate at $z = 4.25$ and a Lyman-limit system at $z = 4.51$. There is absorption in the blue wing of the Lyα emission line that corresponds to Mg II at $z = 1.395$ but no confirming Fe II can be observed due to the Lyα forest. Single absorption lines are observed that could correspond to Si IV and C IV at $z = 3.91$ and C IV at 4.25. C IV doublets are seen at $z = 3.422$, 3.571, and 3.589. There is an Mg II doublet at $z = 1.794$.

5.17. *BR 1117−1329* ($z_{\rm em} = 3.958$, BAL)

This QSO exhibits broad absorption lines for O VI, N V, Si IV, and C IV at $z = 3.62$ and 3.89.

5.18. *BR 1144−0723* ($z_{\rm em} = 4.147$, BAL)

This object exhibits broad absorption lines but also has detectable intervening absorption. There is a strong broad absorption trough corresponding to C IV and a weak trough for Si IV at $z = 4.00$. The emission lines are weak. There is a damped Lyα candidate system at $z = 3.26$, but this is probably confused with broad O VI absorption at $z = 4.0$. There is Mg II absorption at $z = 1.905$ and five corresponding Fe II lines.

5.19. *BR 1202−0725* ($z_{\rm em} = 4.694$)

This is the highest redshift and brightest object in the APM sample. It has very weak emission lines with Lyα and C IV almost completely absorbed away. The spectrum is very similar to that of BRI 1335−0417, described below. The redshift is determined from the edge of the Lyα emission line since the metal lines are so heavily absorbed. (The redshift determined from O I and C IV is 4.679.) There is a damped Lyα system at $z = 4.38$ and a Lyman-limit system at $z = 4.52$. Mg II doublets, some with associated Fe II, are observed at $z = 1.463$, 1.754, 2.238, 2.339, and 2.444. C IV is detected at $z = 3.525$, 3.565, 4.474, and 4.679. See Wampler et al. (1996) for a detailed analysis of the Lyα forest in this object.

5.20. *BR 1302−1404* ($z_{\rm em} = 3.996$, BAL)

This QSO exhibits a complex series of broad absorption lines for OVI, N V, Si IV, and C IV at $z \approx 3.65$, 3.72, and 3.92. There are two Mg II doublets at $z = 2.044$ and 2.058 with four and three associated Fe II lines, respectively.

5.21. *BRI 1328−0433* ($z_{\rm em} = 4.217$)

The OVI, Lyα , N V, Si IV + O IV], and C IV emission lines are strong with weaker O I present. This is one of the few objects in the sample with well-defined N V emission. There is strong Mg II absorption at $z = 1.628$ with two Fe II lines. Lyman-limit systems are seen at $z = 3.31$ and 4.25.

5.22. *BRI 1335−0417* ($z_{\rm em} = 4.396$)

The Lyα + N V and C IV emission lines are very weak, with the Lyα almost completely absorbed away. This QSO looks very similar to BR 1202−0725. Mg II, with four associated Fe II lines, is seen at $z = 1.822$. There is a Lyman-limit system at $z = 4.45$ and Si II and C II at $z = 4.40$. There is strong Lyα absorption at the QSO redshift.

5.23. *BRI 1346−0322* ($z_{\rm em} = 3.992$)

The Lyα and C IV emission lines are very strong and sharp. There is N V absorption at $z = 3.974$. There are C IV doublets at $z = 3.359$ and 3.994, and a single line that is most likely C IV at $z = 3.974$. Mg II with Fe II is seen at $z = 1.944$. There is a damped Lyα candidate at $z = 3.73$ and a corresponding Lyman-limit absorption edge at $z = 3.75$.

5.24. *BRI 1500+0824* ($z_{\rm em} = 3.943$)

The Lyα + N V, O I, Si IV + O IV], and C IV emission lines are weak but sharp. There is a damped Lyα candidate at $z = 2.80$, Mg II with six Fe II lines at $z = 1.908$, and C IV absorption in the emission line at $z = 3.940$. This object shows one of the most successful removals of the O_2 A-band absorption at 7600 Å, in the middle of the C IV emission.

5.25. *GB 1508+5714* ($z_{\rm em} = 4.283$)

This is a radio-selected object from Hook et al. (1995). The Lyα and C IV emission lines are strong and sharp. There is a Lyman-limit system at $z = 3.9$.

5.26. *MG 1557+0313* ($z_{\rm em} = 3.891$)

This is a radio-selected object from McMahon et al. (1996). The Lyα and C IV emission are strong and sharp. There is C IV absorption at $z = 3.898$.

5.27. *GB 1745+6227* ($z_{\rm em} = 3.901$)

This is a radio-selected object from Hook et al. (1995), also discovered independently by Becker, Helfand, & White (1992) on the basis of its X-ray emission. The Lyα and C IV emission are strong and sharp. It has Mg II absorption at $z = 1.471$. There are six Fe II lines at $z = 2.322$, but the corresponding Mg II doublet is not seen as it should occur at 9296 Å, redward of the end of this spectrum.

5.28. *BR 2212−1626* ($z_{\rm em} = 3.990$)

The Lyα + N V and C IV emission lines are strong and sharp with weaker O I, Si IV + O IV], and N IV].

5.29. *BRI 2235−0301* ($z_{\rm em} = 4.249$, BAL)

This QSO is the highest redshift BAL in the sample and has very broad absorption troughs. The emission lines are almost completely absorbed, making it difficult to determine an accurate redshift. It exhibits broad absorption lines of O VI ($z = 4.08$), N V ($z = 3.74$), Si IV ($z = 3.83$), and C IV ($z = 3.65$, 3.82, 4.03). There is a possible Mg II doublet at $z = 1.873$.

5.30. *BR 2237−0607* ($z_{\rm em} = 4.558$)

The Lyα + N V, O I, Si IV + O IV], and C IV emission are strong, with the Lyα line being particularly sharp. There is a damped Lyα candidate at $z = 4.08$ and a Lyman-limit system at $z = 4.28$. There is a N V doublet at $z = 4.545$, Si IV at $z = 4.079$, C II at $z = 4.078$, C IV at $z = 4.482$, Fe II at $z = 2.155$, and Mg II at $z = 1.672$.

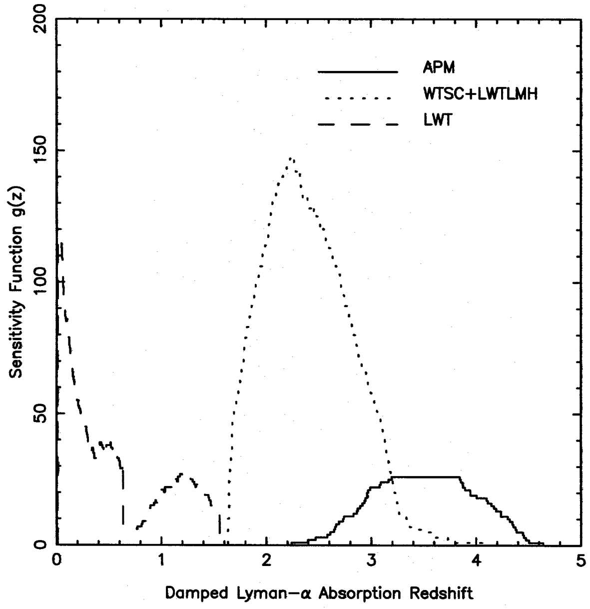

FIG. 6.—The sensitivity function, $g(z)$, of the damped Lyα absorber surveys. This gives the number of lines of sight along which a damped system at redshift z could be detected. The APM survey adds substantial redshift path for $z > 3$.

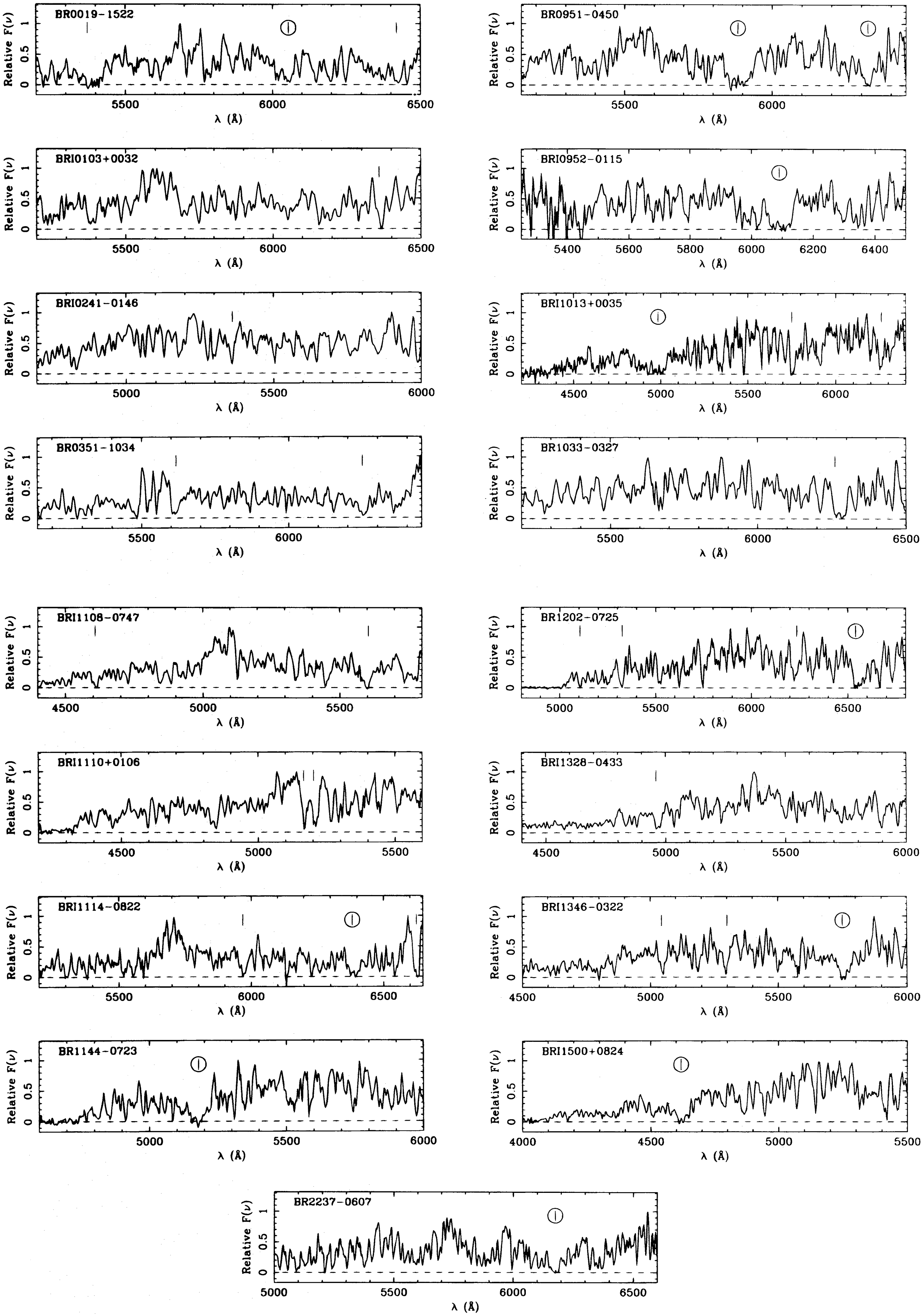

FIG. 7.—The Lyα absorbers listed in Table 7 are marked with a vertical slash in the spectra in this figure. It shows the Lyα forest region on an expanded scale for the QSOs shown in Fig. 4 in which an absorber was measured. The damped Lyα candidates with estimated column densities above the threshold of log $N_{\mathrm{H\,I}} \geq 20.3$ are denoted by footnote *b* after the column density in Table 7 and a circle around the vertical slash in the figure.

5.31. *BR 2248−1242* ($z_{\rm em} = 4.161$)

This QSO has pathologically strong emission lines for O VI + Lyβ, Lyα, N V, O I, C II, Si IV + O IV], N IV], C IV, He II, and O III]. It is the only object with obvious N IV].

6. SURVEY FOR DAMPED Lyα ABSORPTION SYSTEMS

6.1. *Background*

While the baryonic content of spiral galaxies that are observed in the present epoch is concentrated in stars, in the past this must have been in the form of gas. The principal gaseous component in spirals is neutral hydrogen, which has led to surveys for absorption systems detected by the damped Lyα (DLA) lines they produce (Wolfe et al. 1986, 1995; Lanzetta et al. 1991, 1995). Damped Lyα absorption systems comprise the high column density tail of neutral hydrogen absorbers with column densities of $N_{\rm HI} \geq 2 \times 10^{20}$ cm^{-2}. They are identified by the presence of broad (FWHM > 5 Å) absorption lines shortward of Lyα (1216 Å) in the QSO rest frame. These lines are broadened by radiation damping and at $z > 4$ have observed equivalent widths of $W \gtrsim 25$ Å. The visibility of the damping wings in the absorption profile is due to the large H I column density and the low-velocity dispersion (~ 10 km s^{-1}), two features that damped systems have in common with spiral galaxies observed at the present. The column density along a typical line of sight in the Milky Way is $N_{\rm H\,I} \sim 10^{21}$ atoms cm^{-2}. Other features that resemble H I disk galaxies are the presence of metals in mainly low-ionization states such as C+, Si+, and Fe+ and the detection of 21 cm absorption associated with damped systems shows that the gas is cold and has a low level of turbulence (c.f. Wolfe et al. 1986; Wolfe 1987; Turnshek et al. 1989).

6.2. *Selection of Damped Lyα Candidates*

The Lyα forest region in QSO spectra at redshift 4 is very crowded. Many lines are blended at 5 Å resolution and may appear broader than they actually are. However, real damped absorbers at high redshift result in very broad lines. They have observed equivalent widths $W > 25$ Å and are relatively easy to see in the spectra. Two techniques were used to select the candidate absorbers. We first selected the candidates interactively and then independently used the standard equivalent width selection criteria with an automated algorithm. There was good agreement between the two selection methods, although we report only the candidates selected with the automated algorithm. This is described below.

The technique used for selecting candidates and measuring the sensitivity of the survey with redshift follows the methods used in Lanzetta et al. (1991) and is described below. A local continuum was fitted to each spectrum using straight lines between the peaks of the forest regions. An equivalent width spectrum and variance spectrum were created for each QSO defined as

$$W_i = \Delta\lambda \sum_{n=i-m}^{i+m} (1 - F_n/C_n) ,$$

$$\sigma_{E_i}^2 = (\Delta\lambda)^2 \sum_{n=i-m}^{i+m} (\sigma_{F_n}/C_n)^2 ,$$

where C_i and F_i are the continuum and flux levels at pixel i, $\Delta\lambda$ is the angstrom per pixel of the spectrum, and $2m + 1$ is the passband over which the total equivalent width is measured. A passband of 15 pixels was used, equivalent to 37.5 Å.

The spectra were analyzed using the above algorithm starting 3000 km s^{-1} blueward of the emission redshift to avoid lines possibly associated with the quasar. The analysis was stopped when the signal-to-noise ratio became too low to detect a Lyα line with W(rest) ≥ 5 Å at the 5 σ level. This point was typically caused by the incidence of a Lyman limit system. This selected wavelength range is used to construct the sensitivity function, $g(z)$. It gives the number of lines of sight at a given redshift over which damped systems can be detected at a higher than 5 σ level (see Lanzetta et al. 1991 or 1995). Figure 6 shows the sensitivity function of the APM survey compared with three previous damped Lyα surveys (Wolfe et al. 1986; Lanzetta et al. 1991, 1995). The APM survey adds substantial redshift path for damped Lyα absorption system surveys, more than trebling the path surveyed for $z > 3$. The redshift path over which damped systems could be detected is crucial in estimating the cosmological mass density in neutral gas from the damped systems (Storrie-Lombardi et al. 1996b). Gaussians were fitted to the lines selected by the algorithm, and $N_{\rm H\,I}$ was estimated for features with $W > 20$ Å. Of the 32 measured, 11 have estimated $N_{\rm H\,I} \geq 2 \times 10^{20}$ cm^{-2} covering $2.8 \leq z \leq 4.4$. Only one candidate has estimated $N_{\rm H\,I} \geq 10^{21}$ cm^{-2}. They are all listed in Table 7 along with the QSOs with no candidates detected above this threshold. The absorbers listed in Table 7 are marked with a vertical slash in the spectra in Figure 7. The damped Lyα candidates

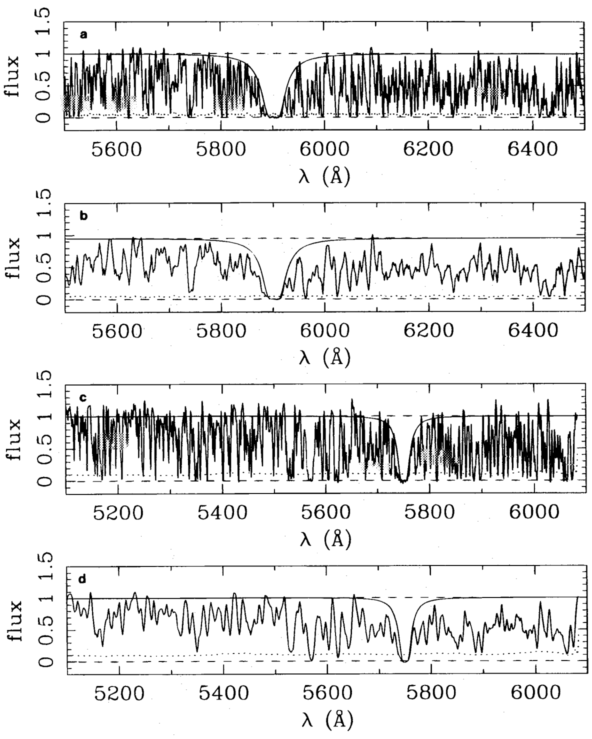

FIG. 8.—Two simulated QSOs with absorbers are shown. Panels (*a*) and (*b*) show a $z = 3.86$, log $N_{\rm H\,I} = 20.69$ damped Lyα absorption system in a $z = 4.37$ QSO at 1.6 and 6 Å resolution, respectively, with a signal-to-noise ratio of 25. Panels (*c*) and (*d*) show a $z = 3.73$, log $N_{\rm H\,I} = 20.15$ Lyα absorption system in a $z = 4.51$ QSO at 1.6 and 6 Å resolution, respectively, with a signal-to-noise ratio of 10.

1996ApJ...468..121S

TABLE 7

APM DAMPED LYα ABSORPTION SURVEY

QSO	$z_{\rm min}$	$z_{\rm max}$	$z_{\rm em}$	Metals[a]	$z_{\rm abs}$	$W_{\rm rest}$ (Å)	log $N_{\rm H\,I}$ Estimated
BR 0019 − 1522.......	2.97	4.473	4.528	Si II 1526, Fe II 1608	3.42	7.6	20.0
	...	...	...	C IV 1549	...	...	...
	...	...	...	...	3.98	12.3	20.5[b]
	...	...	...	...	4.28	8.0	20.1
BRI 0103+0032	2.87	4.383	4.437	...	4.23	5.8	19.8
BRI 0151 − 0025......	2.74	4.142	4.194	...	...	...	...
BRI 0241 − 0146......	2.86	4.002	4.053	...	3.41	5.7	19.8
BR 0245 − 0608.......	2.96	4.186	4.238	...	...	...	...
BR 0351 − 1034.......	3.09	4.297	4.351	C IV 1549	3.62	6.6	19.9
	...	...	...	...	4.14	6.3	19.9
BR 0401 − 1711.......	2.82	4.184	4.236	...	...	...	...
BR 0951 − 0450.......	2.93	4.315	4.369	Si IV 1400, C IV 1549	3.84	24.0	21.0[b]
	...	...	...	Si II 1526	...	...	...
	...	...	...	...	4.20	10.6	20.3[b]
BRI 0952 − 0115......	2.99	4.372	4.426	C II 1334, C IV 1549	4.01	18.0	20.8[b]
	...	...	...	Si IV 1400, Si II 1526	...	...	...
BRI 1013+0035	2.61	4.351	4.405	Fe II 1608	3.10	17.5	20.8[b]
	...	...	...	...	3.73	9.6	20.2
	...	...	...	...	4.15	7.4	20.0
BR 1033 − 0327.......	2.91	4.454	4.509	C II 1334	4.15	9.6	20.2
BRI 1050 − 0000......	2.83	4.233	4.286	...	...	...	...
BRI 1108 − 0747......	2.64	3.873	3.922	...	2.79	8.3	20.1
	...	...	...	C IV 1549	3.61	9.0	20.2
BRI 1110+0106	2.58	3.869	3.918	...	3.25	5.2	19.7
	...	...	...	...	3.28	6.2	19.9
BRI 1114 − 0822......	3.19	4.440	4.495	...	3.91	6.7	19.9
	...	...	...	...	4.25	11.7	20.4[b]
	...	...	...	...	4.45	5.3	19.7
BR 1144 − 0723[c]......	2.89	4.096	4.147	...	3.26	17.8	20.8[b]
BR 1202 − 0725.......	3.16	4.637	4.694	...	3.20	5.4	19.7
		...	...	...	3.38	7.1	20.0
	...	...	...	...	4.13	7.8	20.1
	...	...	...	C II 1334	4.38	13.2	20.5[b]
BRI 1328 − 0433......	2.24	4.165	4.217	...	3.08	8.3	20.1
BRI 1335 − 0417......	3.08	4.342	4.396	...	...	...	...
BRI 1346 − 0322......	2.65	3.942	3.992	...	3.15	6.8	19.9
	...	...	...	C IV 1549	3.36	5.0	19.7
	...	...	...	...	3.73	10.0	20.3[b]
BRI 1500+0824	2.39	3.894	3.943	Fe II 1608, Al II 1671	2.80	11.3	20.4[b]
GB 1508+5714	2.73	4.230	4.283	...	...	...	...
MG 1557+0313	2.66	3.842	3.891	...	...	...	...
GB 1745+6227	2.47	3.852	3.901	...	...	...	...
BR 2212 − 1626.......	2.69	3.940	3.990	...	...	...	...
BR 2237 − 0607.......	2.96	4.502	4.558	C II 1334, Si IV 1400	4.08	11.5	20.4[b]
BR 2248 − 1242.......	2.94	4.109	4.161	...	...	...	...

NOTE.—$z_{\rm min}$ = minimum redshift at which a DLA could be observed; $z_{\rm em}$ = emission redshift of the QSO; $z_{\rm max}$ = 3000 km s^{-1} blueward of $z_{\rm em}$; $z_{\rm abs}$ = redshift at which a DLA candidate was observed.

[a] Metals detected (see Table 5) that correspond to the damped candidate redshift.

[b] These candidates are above the statistical sample threshold of $N_{\rm H\,I} \geq 2 \times 10^{20}$ atoms cm^{-2}.

[c] This QSO exhibits some BAL characteristics. The damped candidate at $z = 3.26$ is tentative as it falls at the same wavelength as O VI at $z = 4.0$.

with estimated column densities above the threshold of log $N_{\rm H\,I} \geq 20.3$ are denoted by footnote b in Table 7 and by a circle around the vertical slash in Figure 7.

To test this selection procedure, simulated high-resolution spectra with damped systems included at known column densities were degraded to 6 Å resolution and the column densities estimated with the above technique. The estimates were within $\pm 0.2 \times 10^{20}$ atoms cm^{-2} of the real value. Two simulated QSOs are shown in Figure 8. Figures 8*a* and 8*b* show a $z = 3.86$, log $N_{\rm H\,I} = 20.69$ damped Lyα absorption system in a $z = 4.37$ QSO at 1.6 and 6 Å resolution, respectively, with a signal-to-noise ratio of 25. Figures 8*c* and 8*d* show a $z = 3.73$, log $N_{\rm H\,I} = 20.15$ Lyα absorption system in a $z = 4.51$ QSO at 1.6 and 6 Å resolution, respectively, with a signal-to-noise ratio of 10.

Many of the damped candidates have estimated $N_{\rm H\,I}$ near the statistical sample threshold of $N_{\rm H\,I} = 2 \times 10^{20}$ atoms cm^{-2} (Wolfe et al. 1986). Some of those with $N_{\rm H\,I} < 2 \times 10^{20}$ will be confirmed as damped, and some of those with $N_{\rm H\,I} \geq 2 \times 10^{20}$ will turn out to be blends of weaker lines. Higher resolution spectra are essential to verify the individual column densities, although the estimates should give an accurate representation of their distribution at high redshift. Three of the candidates have been observed at ESO with the NTT, and these are discussed in Storrie-Lombardi et al. (1996a). Preliminary results from 1.5 Å resolution spectra taken with LRIS on the Keck telescope indicate that the rest of the candidates selected are representative of the true distribution of H I column densities at high redshift (Storrie-Lombardi & Wolfe 1996). When the follow-up spectroscopy is complete, this will result in a complete sample of damped absorbers for $z > 3.5$, increasing the confirmed numbers of these absorbers by $\sim 20\%$ and covering an epoch crucial to understanding the formation of galaxies.

7. CONCLUSIONS

Intermediate-resolution (5 Å) spectrophotometry is presented for 31 QSOs with redshifts $3.9 \leq z \leq 4.7$, 28 from the APM Color Survey and three radio-selected objects. The spectra were surveyed to create new data sets of intervening absorption lines systems. The QSOs display a wide variety of emission and absorption line characteristics, with five exhibiting broad absorption lines and one with extremely strong emission lines (BR 2248−1242).

This high-redshift data set more than triples the $z > 3$ redshift path available for damped Lyα absorption system surveys. Eleven candidate damped systems have been identified covering the redshift range $2.8 \leq z \leq 4.4$ (eight with $z > 3.5$). The redshift evolution, column density distribution function, and contribution to the cosmological mass density from these systems is discussed in other papers (Storrie-Lombardi et al. 1996a, 1996b).

The Lyman-limit systems in the QSOs with $z \geq 4.2$ are cataloged and the spectra presented. Their redshift evolution has been discussed in a previous paper (Storrie-Lombardi et al. 1994). In addition, line lists for metal absorption-line systems (e.g., C IV and Mg II) are presented. An analysis of the measured redshifts of the high-ionization emission lines with the low-ionization lines shows them to be blueshifted by 430 ± 60 km s^{-1}.

We thank an anonymous referee and Mike Fall for suggestions that improved the paper and Art Wolfe for the use of his code in the automated damped candidate selection. We thank the PATT for time awarded to do the observations with the William Herschel Telescope that made this work possible. L. S. L. acknowledges support from an Isaac Newton Studentship, the Cambridge Overseas Trust, and a University of California President's Postdoctoral Fellowship. R. G. M. acknowledges the support of the Royal Society.

REFERENCES

Bajtlik, S., Duncan, R. C., & Ostriker, J. P. 1988, ApJ, 327, 570

Becker, R. H., Helfand, D. J., & White, R. L. 1992, ApJ, 104, 531

Carswell, R. F., et al. 1991, ApJ, 381, L5

Carswell, R. F., Webb, J. K., Baldwin, J. A., & Atwood, B. 1987, ApJ, 319, 709

Efstathiou, G., & Rees, M. J. 1988, 230, 5P

Espey, B. R., Carswell, R. F., Bailey, J. A., Smith, M. G., & Ward, M. J. 1989, ApJ, 342, 666

Fall, S. M., Pei, Y. C., & McMahon, R. G. 1989, ApJ, 341, L5

Filippenko, A. V. 1982, PASP, 94, 715

Hayes, D. S., & Latham, D. W. 1975, ApJ, 197, 593

Hirshfeld, A., Sinnott, R. W., & Ochsenbien, F. 1991, Sky Catalogue 2000.0 (Cambridge: Cambridge Univ. Press)

Hoffleit, D., & Jaschek, C. 1982, Bright Star Catalogue (New Haven: Yale Univ. Obs.)

Hook, I. M., McMahon, R. G., Patnaik, A. R., Browne, W., Wilkinson, P. N., Irwin, M. J., & Hazard, C. 1995, MNRAS, 273, L63

Hunstead, R. W., Murdoch, H. S., Peterson, B. A., Blades, J. C., Jauncey, D. L., Wright, A. E., Pettini, M., & Savage, A. 1986, ApJ, 305, 496

Irwin, M. J., McMahon, R. G., & Hazard, C. 1991, in ASP Conf. Ser., Vol. 21, The Space Distribution of Quasars, ed. D. Crampton (San Francisco: ASP), 117

Irwin, M. J., et al. 1996, in preparation

Lanzetta, K. M. 1991, ApJ, 375, 1

Lanzetta, K. M., Wolfe, A. M., & Turnshek, D. A. 1995, ApJ, 440, 435

Lanzetta, K. M., Wolfe, A. M., Turnshek, D. A., Lu, L., McMahon, R. G., & Hazard, C. 1991, ApJS, 77, 1

McMahon, R. G., et al. 1996, in preparation

McMahon, R. G., Irwin, M. J., & Hazard, C. 1992, Gemini Issue, 36, 1

McMahon, R. G., Omont, A., Bergeron, J., Kreysa, E., & Haslam, C. G. T. 1994, MNRAS, 267, L9

Oke, J.B. 1969, PASP, 81, 11

———. 1974, ApJS, 27, 21

Oke, J. B., & Gunn, J. E. 1983, ApJ, 266, 713

Pettini, M., Boksenberg, A., & Hunstead, R. W. 1990, ApJ, 348, 48

Rauch, M., Carswell, R. F., Robertson, J. G., Shaver, P. A., & Webb, J. K. 1990, MNRAS, 242, 698

Sargent, W. L. W., Steidel, C. C., & Boksenberg, A. 1989, ApJS, 79, 703

Steidel, C. C., & Sargent, W. L. W. 1991, ApJ, 382, 433

Stengler-Larrea, E. A., et al. 1995, ApJ, 444, 64

Storrie-Lombardi, L. J., et al. 1997, in preparation

Storrie-Lombardi, L. J., Irwin, M. J., & McMahon, R. G. 1996a, MNRAS, in press

Storrie-Lombardi, L., McMahon, R. G., & Irwin, M. J. 1996b, MNRAS, submitted

Storrie-Lombardi, L. J., McMahon, R. G., Irwin, M. J., & Hazard, C. 1994, ApJ, 427, L13

Storrie-Lombardi, L. J., & Wolfe, A. M. 1996, in preparation

Turnshek, D. A., Wolfe, A. M., Lanzetta, K. M., Briggs, F. H., Cohen, R. D., Foltz, C. B., Smith, H. E., & Wilkes, B. J. 1989, ApJ, 344, 567

Tytler, D., & Fan, X. M. 1992, ApJS, 79, 1

Wampler, E. J., Williger, G. M., Baldwin, J. A., Carswell, R. F., Hazard, C., & McMahon, R. G. 1996, A&A, in press

White, R. L., & Becker, R. H. 1992, ApJS, 79, 331

Williger, G. M., Baldwin, J. A., Carswell, R. F., Cooke, A. J., Hazard, C., Irwin, M. J., McMahon, R. G., & Storrie-Lombardi, L. J. 1994, ApJ, 428, 574

Wolfe, A. M. 1987, Proc. Phil. Trans. Roy. Soc., 320, 503

Wolfe, A. M., Lanzetta, K. M., Foltz, C. B., & Chaffee, F. H. 1995, ApJ, 454, 698

Wolfe, A. M., Turnshek, D. A., Smith, H. E., & Cohen, R. D. 1986, ApJS, 61, 249